Co-Aromatization of Olefin and Methane over Ag-Ga/ZSM-5 Catalyst at Low Temperature

Peng He[1], Richard Gatip[1], Matthew Yung[2], Hongbo Zeng[3], Hua Song[1]*

[1]Department of Chemical and Petroleum Engineering, University of Calgary, 2500 University Dr NW, Calgary, Alberta T2N 1N4, Canada

[2]National Bioenergy Center, National Renewable Energy Laboratory, 15013 Denver West Parkway, Golden, Colorado 80401, United States of America

[3]Department of Chemical and Materials Engineering, University of Alberta, 9211-116 Street NW, Edmonton, Alberta T6G 1H9, Canada

*Corresponding author

Fax: +1 (403) 284-4852; Tel: +1 (403) 220-3792;

E-mail: sonh@ucalgary.ca

Pursuant to the DOE Public Access Plan, this document represents the authors' peer-reviewed, accepted manuscript. The published version of the article is available from the relevant publisher.

Abstract

The massive exploitation of shale gas in the past decade has boosted the production of natural gas and reduced its price dramatically. The methane activation and following conversion into more valuable fuels and chemicals have thus become more and more attractive, while the introduction of hydrocarbons to enhance the methane activation at mild conditions represents a promising approach. In the present work, the co-aromatization of methane with propylene has been studied at 400 ^{o}C. The presence of methane would increase the toluene to benzene ratio as well as the average carbon number of the formed liquid aromatic products compared to its propylene alone counterpart. Among the gas products, the formations of C_3H_8, C_4H_8 and C_4H_{10} also get promoted when methane is present. The incorporation of methane into the product molecules is also directly evidenced by the ^{1}H, ^{2}D and ^{13}C NMR spectroscopy of the liquid products obtained from the reaction between propylene (or styrene) and isotope labelled methane. Hydrogen from methane would contribute a large portion of the hydrogen in the product molecules, while the benzylic and aromatic hydrogen sites are favored compared with those on the alkyl side chains. The activation of methane is also observed in the DRIFT spectra when deuterium enriched methane is engaged as the methane source and evidenced by the escalated exothermic feature when olefin aromatization takes place under methane environment. The excellent catalytic performance of Ag-Ga/ZSM-5 might be because of the better dispersion of Ag and Ga on the ZSM-5 surface and moderate amount of strong Brösted and Lewis surface acid sites. All the observations suggest that methane might be activated nonoxidatively and converted into aromatics if suitable catalyst is charged under the assistance of co-existing olefin. The reported synergetic effect could potentially lead to the more economic utilization of abundant natural gas and petrochemical intermediates.

Keywords: Methane activation; Aromatization; ZSM-5; Olefin; Catalyst

Pursuant to the DOE Public Access Plan, this document represents the authors' peer-reviewed, accepted manuscript. The published version of the article is available from the relevant publisher.

1. Introduction

The past decade has witnessed greatly changed landscape of energy industry due to the recent discoveries of large reserves of natural gas, i.e., shale gas, and the breakthroughs made in the exploitation technology. According to the data released by US Energy Information Administration, the production of natural gas is averaged 49.6 billion cubic feet per day (BCF/d) in 2006, which is increased to 79.0 BCF/d in January 2016. The price of Henry Hub natural gas in US has dropped from $12.28 in the last quarter of 2005 to $1.73 per million Btu (MBTU) in March 2016. However, the utilization of natural gas is limited by the difficulty in its liquefaction. The transportation of natural gas relies heavily on pipelines. And its application is often restricted to combustion in heating systems rather than vehicle fuels. The inert molecular structure of methane, the principal component of natural gas, also dents its application as chemical feedstocks. Methane has to follow multistep conversion strategies via syngas and/or methanol before its transformation into higher hydrocarbons, resulting in increased cost and thus impeding its commercial potential. In 2015, the price of Henry Hub natural gas in US is averaged US $2.77 per MBTU, while that of West Texas Intermediate (WTI) light sweet crude oil is averaged US $48.79 per barrel, which is equivalent to US $8.79 per MBTU. The greatly underestimated value of methane has driven researchers to search for ways to boost the profitability of the natural gas industry, especially during the current era of low energy prices. The conversion of low cost methane into high value added commodities including more commercially useful chemicals and liquid fuels has attracted great attention in recent years. However, methane is the most inert hydrocarbon molecules due to its highly symmetric molecular structure and high C-H bond energy of 435 kJ/mol, which is the highest among all naturally available hydrocarbons, making the effective activation and direct conversion of methane become one of the great challenges faced by the entire catalysis field. Oxidative

Pursuant to the DOE Public Access Plan, this document represents the authors' peer-reviewed, accepted manuscript.
The published version of the article is available from the relevant publisher.

coupling of methane to produce ethylene has been extensively studied to convert methane into more valuable chemicals since 1980s. Hundreds of catalyst systems focusing on converting methane into ethylene, an important feedstock in petro-chemistry, have been synthesized and comprehensively reviewed.[1–3] But the low yield of C_2 hydrocarbons, which is often below 25%, dents its industrial application. The highly exothermic hydrocarbon oxidation reactions in this process may also induce undesirable products such as CO and CO_2. Converting methane into methanol under oxidative environment is also a challenging task in terms of selectivity since the C-H bonds of the product are more reactive than that of methane.[4] As a result, an increased methane conversion comes with the loss of the selectivity. Therefore, methane is first converted into syngas by reforming process before its transformation into methanol and gasoline rather than direct conversion into liquid hydrocarbons in industrial practices.[5] On the other side, the direct transformation of methane into liquid chemicals such as aromatics has been numerously explored under non-oxidative environment. Many catalysts have been reported[6–14] in the past decades, but the application of this approach is also impeded by the low yield and high reaction temperature, which is often above 700 ^{o}C and may exceed 1000 ^{o}C in certain occasions. Nonetheless, Choudhary *et al*[15] achieved effective activation and conversion of methane over H-galloaluminosilicate ZSM-5 type zeolite at lower temperature regions of 500-600 ^{o}C by the addition of higher hydrocarbons in the feed. This approach is also evidenced by a series of succeeding publications[5,16–22] demonstrating that the conversion of methane would be significantly enhanced when methane was co-fed with hydrocarbons, such as ethylene, propylene, pentane, hexane, light gasoline, liquefied petroleum gas, and even oxygenated hydrocarbons like methanol and ethanol. These observations have shed light on the methane conversion promoted by the presence of higher hydrocarbons.

Pursuant to the DOE Public Access Plan, this document represents the authors' peer-reviewed, accepted manuscript.
The published version of the article is available from the relevant publisher.

The study on the liquid products obtained from aforementioned methane conversion, however, is rare, which might be because the research on methane conversion is often focused on the gas phase products. Over the past decade, lots of efforts have been devoted to the mechanistic study on the methane activation. One powerful method is to probe the surface species evolution on the catalyst by solid-state NMR spectroscopy at variable temperatures when methane or the mixture of methane and higher hydrocarbon is introduced to the catalyst[21,23–26], which provides some insight into the methane activation and initial reaction intermediates. But these experiments are often carried out under vacuum conditions in order to remove unreacted gas feedstocks before acquiring the ^{13}C NMR spectra of the organic species adsorbed on the catalyst. Therefore the extent of the reaction and methane conversion cannot be accurately evaluated for potential industrial application, which is often executed at higher pressures. More detailed information in terms of the distribution of the carbon and hydrogen from methane in the liquid product molecules is thus necessary for a better understanding of the reaction mechanism.

Under such background, this paper studies the technical feasibility of co-aromatization of methane with propylene over Ag-Ga/ZSM-5 catalyst at a low temperature of 400 ^{o}C. The compositional distribution of the formed gaseous and liquid products and the heat effect of the reaction are studied to investigate the participation of methane. The incorporation of methane into the liquid products is directly evidenced by the ^{13}C and ^{2}D isotope labelling method, which also helps revealing the reaction mechanism. The engaged catalyst is then systematically characterized to identify the relationship between the properties and its corresponding performance towards co-aromatization of methane and propylene.

Pursuant to the DOE Public Access Plan, this document represents the authors' peer-reviewed, accepted manuscript.
The published version of the article is available from the relevant publisher.

2. Experimental

2.1 Catalyst Synthesis

NH_4-ZSM-5 with a SiO_2/Al_2O_3 ratio of 80:1 was obtained from Zeolyst USA. The zeolite was converted into H-ZSM-5 through calcination at 600 ºC in ambient air for 5 h. The metal-modified HZSM-5 was prepared by wetness impregnation method. 0.13 g $AgNO_3$ (Alfa Aesar, 99.9%) and 0.30 g $Ga(NO_3)_3 \cdot xH_2O$ (99.9%, Alfa Aesar) were dissolved into 10 g deionized (DI) water to form the aqueous solution of the metal precursor, which was then impregnated to 8.0 g H-ZSM-5 for preparing 1%Ag-1%Ga/ZSM-5. The obtained wet powder was dried in the oven at 92 ºC overnight, followed by calcination at 600 ºC for 3 h in ambient air.

2.2 Catalytic performance evaluation

The olefin upgrading reaction was carried out in a 100 mL batch reactor manufactured by Parr Instrument that could tolerate high temperature up to 500 ºC and high pressure up to 350 bar. In a typical run, 0.5 g Ag-Ga/ZSM-5 were put into the reactor, which was then purged and filled with 0.2 MPa propylene, followed by the introduction of methane to the total pressure of 1.0, 3.0, 5.0 and 7.0 MPa. The reactor temperature was then ramped up with a rate of 20 ºC/min to the destination temperature (400 ºC) and held for 60 mins. Upon the reaction completion, the reactor was allowed to cool down to room temperature before product collection. The gas product was first discharged to a 2.2 L cylinder, which was previously purged by N_2. The gas temperature and pressure (60-450 kPa) within the cylinder were then recorded before the gas product was analyzed by a connected micro-GC. The formed liquid product embedded into the charged solid catalyst was extracted out using 10.0 g CS_2 (GC grade, EMD Chemicals) as solvent and internal standard for following NMR analysis.

Reaction between propylene and $^{13}CH_4$ and CD_4 (99.9% ^{13}C and 99% ^{2}D, respectively,

Pursuant to the DOE Public Access Plan, this document represents the authors' peer-reviewed, accepted manuscript.
The published version of the article is available from the relevant publisher.

Cambridge Isotope Laboratories, Inc.) were also conducted in a similar manner when 0.5 g catalyst was charged. The reactor was pressured to 0.3 MPa by $^{13}CH_4$ or CD_4 after being filled with 0.2 MPa propylene. When styrene (≥99%, Sigma Aldrich) was employed as the feedstock, a glass vial carrying 0.1 g styrene was put into the reactor which was purged by N_2 and pressurized to 0.2 MPa using $^{13}CH_4$ or CD_4 before the reaction was carried out.

The composition of the product oil was determined by the pre-calibrated Gas Chromatography-Mass Spectrometer (GC-MS: PerkinElmer GC Claus 680 and MS Clarus SQ 8T) equipped with a Paraffins-Olefins-Naphthenes-Aromatics (PONA) column (Agilent HP-PONA). The oven temperature of the GC was programmed to hold at 35 ºC for 15 min, ramp to 70 ºC at 1.5 ºC/min, rise to 150 ºC at 3 ºC/min and hold for 30 min, then ramp to 250 ºC at 3 ºC/min and hold for 2 min. The MS spectra of each peak is obtained by averaging the Total Ion Current with respect to m/z value of all the points in this peak.

The gas products were analyzed by the aforementioned four-channel micro-GC (490, Agilent) equipped with thermal conductivity detectors, which can precisely analyze H_2, O_2, N_2, CH_4, and CO in the first channel equipped with a 10 m molecular sieve 5A column; CO_2, C_2H_2, C_2H_4, and C_2H_6 in the second channel installed with a 10 m PPU column; and C_3−C_6 and $C_{3=}$−$C_{5=}$ in the third and fourth channels charged with a 10 m alumina column and a 8 m CP-Sil 5 CB column, respectively. Ar and He were the carrier gases for the first and other three channels, respectively. The composition of the gas products were used to calculate the moles of each species.

The mass of the liquid product is calculated from the mass gain of the reactor after the reaction measured using a Mettler Toledo MS120027S scale with accuracy of ±0.01 g. The carbon and hydrogen balances counting the products in the gas phase and adsorbed on the catalyst surface were conducted after each run with measured closures of 0.94~1.02 and 0.97~1.06, respectively.

Pursuant to the DOE Public Access Plan, this document represents the authors' peer-reviewed, accepted manuscript.
The published version of the article is available from the relevant publisher.

159 The ^{1}H NMR experiments were conducted at 9.4 T ($\nu_0(^{1}H)$ = 400.1 MHz) on a BRUKER
160 AVANCEIII 400 spectrometer with a BBFO probe. ^{1}H NMR chemical shifts were referenced to
161 $CHCl_3$ at 7.28 ppm. A spectral width of 12 kHz and a pulse delay of 3.5 s were used to acquire 64
162 scans per spectrum. The NMR samples in the tubes were prepared by mixing 0.30 mL sample with
163 0.30 mL $CDCl_3$ (99.8% atom D, Sigma). The track amount of $CHCl_3$ in $CDCl_3$ functioned as an
164 internal standard.

165 The ^{2}D NMR experiments were conducted at 9.4 T ($\nu_0(^{2}D)$ = 61.4 MHz) on a BRUKER
166 AVANCEIII 400 spectrometer with a BBFO probe. A spectral width of 2.5 kHz and a recycle delay
167 of 7 s were used to acquire 512 scans per spectrum.

168 The ^{13}C NMR experiments were conducted at 14.1 T ($\nu_0(^{13}C)$ = 150.9 MHz) on a BRUKER
169 AVANCEIII 600 spectrometer using a zgpg30 pulse program. ^{13}C NMR chemical shifts were
170 referenced to $CDCl_3$ at 77.23 ppm. A spectral width of 36 kHz and a recycle delay of 2 s were used
171 to acquire 10000 scans per spectrum. The NMR samples in the tubes were prepared by mixing
172 0.50 mL sample with 0.10 mL $CDCl_3$.

173 Thermographic Analysis (TGA) profiles were used to determine the thermal coke formation as
174 well as the stability of the catalysts. TGA measurement was fulfilled with a simultaneous thermal
175 analyzer (PerkinElmer STA 6000). The samples were held at 50 ^{o}C for 1 min, then ramped to 700
176 ^{o}C at a rate of 10 ^{o}C/min under 30 mL/min air flow. TGA signal along with the simultaneously
177 collected Differential Scanning Calorimetry (DSC) signal were engaged to study the involved
178 reaction features after background correction, which was accomplished through ramping the
179 sample temperature to the destination temperature with a rate of 40 ^{o}C/min under 30 mL/min N_2
180 flow and a hold for 30 min under various gas environments, i.e., 15 mL/min N_2+15 mL/min
181 propylene, 15 mL/min CH_4+15 mL/min propylene, or 30 mL/min CH_4. The thermodynamic

Pursuant to the DOE Public Access Plan, this document represents the authors' peer-reviewed, accepted manuscript.
The published version of the article is available from the relevant publisher.

calculation is carried out using HSC Chemistry 6.1, a chemical reaction and equilibrium software with thermochemical database and simulation module developed by Outotec Research Oy.

2.3 Catalyst characterization

The adsorption and desorption of nitrogen on each catalyst sample, i.e., HZSM-5, fresh Ag-Ga/ZSM-5, spent Ag-Ga/ZSM-5 under CH_4 and N_2 environment at 3 atm, was measured using a Quadrasorb SI from Quantachrome Instruments. Samples were outgassed under a vacuum at 350 °C overnight and then brought to -196 ^oC via immersion in a liquid nitrogen bath. Total surface area was calculated using multi-point Brunauer–Emmett–Teller (BET) analysis. Pore surface area and pore volume were calculated using Barrett–Joyner–Halenda (BJH) analysis. The t-plot method was used with the DeBoer model for the calculation of the statistical thickness to distinguish the contribution of micropores (<2 nm) to the total surface area. The employed modeling methods tend to overestimate the pore size of the microporous materials such as zeolites. This phenomenon has been displayed by BET results from previous publication, where the pore diameter of zeolite beta (6.7 Å) was determined to be 21~67 Å[27].

The crystalline phase compositions of prepared catalysts were examined by X-ray diffraction on a Rigaku Multiflex diffractometer with Cu Kα irradiation at a voltage of 20 kV and current of 40 mA in the 2θ of 5-45^o.

The Transmission Electron Microscopy (TEM) spectra were acquired on a JEOL2200FS TEM instrument operated at 200 kV. An X-ray analyzer for Energy-Dispersive X-ray (EDX) spectroscopy was incorporated into the instrument for elemental analysis using Oxford INCA Energy under STEM mode with 1 nm probe. TEM images were acquired in Bright Field as well as High Angle Annual Dark Field. The sample was first dispersed in ethanol and sonicated for about 2 min. A 10 μL droplet was placed on honey carbon grids before the TEM images were

Pursuant to the DOE Public Access Plan, this document represents the authors' peer-reviewed, accepted manuscript. The published version of the article is available from the relevant publisher.

recorded.

Diffuse Reflectance Infrared Fourier Transform (DRIFT) spectra were acquired by Thermo Scientific Nicolet iS50 equipped with environmental chamber and liquid-nitrogen cooled mercury–cadmium–telluride (MCT) detector. The gas inlet of a multifunctional reactor system fabricated in our research laboratory was employed for the gas introduction to DRIFTS via Fluorinated Ethylene Propylene (FEP) tubing (Thermo Scientific, tubing 890 FEP, 8050-0125). The connection between the FEP tubing and the environmental chamber was accomplished through a short tubing with an inside diameter of 1/4 inch. First, the control group DRIFT spectra were acquired at 512 scans per spectrum with a resolution of 4 cm^{-1}. The catalyst was heated to 500 ^{o}C and held for 30 min under 30 standard cubic centimeters per minute (sccm) N_2 to remove the impurities which might be adsorbed on the catalyst surface during storage. When the catalyst was cooled down to 25 ^{o}C the background spectrum was collected. Then the catalyst was heated up to 100, 200, 300, 400 and 500 ^{o}C, respectively, and the background spectrum at each corresponding temperature was collected. When the catalyst was again cooled to 25 ^{o}C under N_2 environment after background collections, a 30 sccm propylene flow was introduced to the environmental chamber. After that, the gas flow was switched back to 30 sccm pure N_2. The catalyst was held at 25 ^{o}C for 25 min before collecting sample DRIFTS spectrum under Kubelka-Munk mode, and this step was repeated at 100, 200, 300, 400 and 500 ^{o}C, respectively. The DRIFT spectra when CH_4 was present were acquired in a similar manner. The collection of background spectra followed the same procedure. After reactive gas introduction, the gas flow was changed to 30 sccm CH_4 for 10 min followed by 30 sccm N_2 for 15 min before collecting DRIFT spectrum. This step was again repeated at 100, 200, 300, 400 and 500 ^{o}C, respectively, to evaluate the influence of methane presence. Besides CH_4, deuterium enriched methane (CD_4) was also

Pursuant to the DOE Public Access Plan, this document represents the authors' peer-reviewed, accepted manuscript.
The published version of the article is available from the relevant publisher.

228 employed to acquire the spectra in a similar manner.

229 The DRIFT spectroscopy was also engaged to study the surface acidity of the catalyst upon
230 pyridine adsorption at room temperature. The catalyst sample was put in the environmental
231 chamber under 30 sccm N_2 flow. It was first calcined at 500 ^oC for 30 min before collecting
232 background spectra at 25 ^oC. Pyridine was then introduced to the sample by N_2 flow. The spectra
233 were recorded in absorbance mode upon stabilization for 30 min under 30 sccm N_2.

234 Surface acidity measurements were also performed by NH_3 TPD using ~200 mg samples in an
235 Altamira AMI-390 system. Ammonia was selected due to its simplicity, small molecular size, and
236 ability to titrate both strong and weak acid sites on the catalyst. Prior to measurements, fresh
237 samples were activated in 10% O_2/He at 600 °C for 30 min with a ramp rate of 10 °C/min. All
238 samples were then cooled to 160 °C for adsorption of ammonia, performed using a flow of 25
239 sccm of 10% NH_3/He for 30 min. After flowing He for 10 min at 160 ^oC to remove any physically
240 adsorbed NH_3 and cooling to 120 ^oC, TPD was carried out by ramping to 600 °C with at 30 K/min
241 and a hold of 30 min. A thermal conductivity detector (TCD) determined the amount of desorbed
242 NH_3. Upon completion of each experiment, seven pulses of 5 mL of 10 %NH_3/He were used to
243 calibrate the TCD response.

244 X-ray Photoelectron Spectroscopy (XPS) analysis was performed using an AXIS His, 165
245 Spectrometer manufactured by Kratos Analytical with a monochromatized Al Kα X-ray source.
246 2.3V voltage was chosen to make the charge balance. A stainless steel sample holder was used.
247 Survey scans were performed to identify all the elements within the sample, followed by more
248 detailed regional scans for Ag 3d, C 1s, O 1s, and Ga 2p orbitals in order to achieve the high
249 resolution for these elements of interest. A controlled-atmosphere transfer chamber was used for
250 transferring the sample to the XPS instrument without exposure to atmosphere. The binding

Pursuant to the DOE Public Access Plan, this document represents the authors' peer-reviewed, accepted manuscript.
The published version of the article is available from the relevant publisher.

energies were reported relative to C 1s at ~284.8 eV.

3. Results and Discussions

3.1 Catalytic performance

After the reactions between C_3H_6 and methane when Ag-Ga/ZSM-5 catalyst is charged at various pressures, the liquid products are analyzed and determined to be composed of aromatics such as benzene, toluene and C_8 to C_{12} aromatics. Ethyl benzene and xylene are the products observed in C_8 group, among which p-xylene and o-xylene are the major components with the highest population. C_9-C_{12} products include the species with methyl, ethyl, propyl groups, or their combinations attached to benzene and naphthalene as substituent groups, as well as small amount of indene derivatives. The distribution charts of these groups under variable reaction pressures are displayed in Figure 1. At 10 bar toluene and C_8 groups are the primary products. Compared with the control group run, i.e., N_2 environment, the fraction of benzene is lower when CH_4 is present, while the fractions of C_8 and C_9 groups are increased. Such a shift of product distribution toward larger carbon number products might suggest the incorporation of methane into the product molecules. As the reaction pressure is increased to 3.0, 5.0 and 7.0 MPa (Figure 1b, 1c and 1d), the shift of products toward the larger carbon number becomes more prominent, indicating that a higher methane pressure favors the formation of larger product molecules as expected from a thermodynamic calculation. At 7.0 MPa, the primary species in the products are C_8 - C_9 groups (Figure 1d) rather than the C_7-C_8 groups at 1.0 MPa (Figure 1a). Under higher methane pressures, the formation of higher aromatics (C_9-C_{12}), whose kinetic diameters are large compared with the pore size of ZSM-5 framework [28,29] and thus may involve the reaction pathways on the external surface of the catalyst[30,31], becomes more significant. Bijani *et al*[32] demonstrated that when

Pursuant to the DOE Public Access Plan, this document represents the authors' peer-reviewed, accepted manuscript.
The published version of the article is available from the relevant publisher.

methane itself is converted to aromatics and H_2 and a higher pressure would suppress the selectivity of large aromatic molecules such as naphthalene compared with small aromatic molecules such as benzene. In the present work, when olefin is co-fed to react with methane, the product selectivity is shifted to larger aromatic molecules at higher pressures, which might because the reaction pathway network is more complicated than the conversion of sole methane. This phenomenon might also be because the participation of methane during the co-aromatization process under high pressure is more feasible on the external surface of the catalyst. It is also noticed that at higher pressures, the effect on the product distribution in terms of the ratio between toluene and benzene (Figure 2a) and the shift of carbon number (Figure 2b) is enhanced. It is worth noting that the ratio between toluene and benzene gets larger when methane is present, which might be due to the methane participation during the phenyl ring formation. The incorporation of methane into the product molecules is also supported by larger average carbon number under the CH_4 environment.

The gas product composition and the conversion of propylene and methane are displayed in Table 1. It is noticed that as the reaction pressure is increased, the amount of converted methane is promoted, while that of propylene remains almost unchanged. At 1.0, 3.0, 5.0 and 7.0 MPa, the conversions of methane are calculated to be 1.8, 2.3, 4.7% and 3.8 %, and the carbon atoms from methane would contribute 5, 18, 42 and 44 % of the carbon atoms in the product matrix, respectively. Rimer *et al*[33] studied the aromatization reaction of ethylene with and without co-fed methane over Ag-ZSM-5 catalyst at 400 ^{o}C and atmospheric pressure. Despite a lower activation barrier of methane (1.62 eV) on Ag-ZSM-5 than that of ethylene (1.92 eV) according to the DFT calculation, the aromatization process is dominated by ethylene under the given reaction condition. One of the factors that impair the methane conversion is the occupation competition of

Pursuant to the DOE Public Access Plan, this document represents the authors' peer-reviewed, accepted manuscript.
The published version of the article is available from the relevant publisher.

297 Ag^+ Lewis acid sites between methane and ethylene molecules, when the high stability of π-bonded
298 ethylene complex at the Ag^+ site is taken into consideration. These observations give some insights
299 into the reaction pathway of the present work due to the similarity of the reaction matrix. In the
300 presence of co-fed propylene, the reactivity of methane might also be impeded by the propylene
301 π-complex occupying the catalytic sites. This is supported by the observation in the present work
302 that the participation of methane during the reaction is enhanced at higher methane pressures which
303 results in an increased methane concentration. However, the high methane pressure requires a
304 considerable amount of methane in the feed. Since the methane conversion is relatively low (<5%),
305 it is necessary to recycle the unconverted methane feedstock to avoid the waste of methane
306 resources in the future industrial application. Despite the relatively low conversion of methane for
307 commercial application, which might be compensated by the recycling, the feasibility of methane
308 co-aromatization with propylene at 400 ^oC, close to the temperature of petroleum refining
309 processes, opens the door for the application of methane co-aromatization with petroleum
310 feedstocks. It is also observed that the amount of H_2, ethylene and ethane is higher under methane
311 environment, suggesting that their formation may be closely related to the presence of methane.
312 As the reaction pressure is lifted, these species become absent in the product, which may be
313 because H_2 and C_2 products are more readily consumed at high pressures. The GC-MS analysis
314 results show that the formation of alicylic compounds cannot be identified at detectable amount.
315 Two unsaturated aromatic compounds including indene and 4-ethenyl-1,2-dimethylbenzene are
316 detected at the pressures of 1.0 and 3.0 MPa, with a molar percentage of 0.1%. At lifted pressures
317 such as 5.0 and 7.0 MPa, these products as well as H_2 (Table 1) are absent, suggesting that higher
318 pressures would improve the saturation of carbon double bonds. Similarly, the presence of methane
319 also raises the amount of C_4H_8 and C_4H_{10}, probably indicating the participation of methane in the

Pursuant to the DOE Public Access Plan, this document represents the authors' peer-reviewed, accepted manuscript.
The published version of the article is available from the relevant publisher.

formation of C_4 products. It is also worth noting that C_4H_8 is only present under CH_4 environment. A plausible explanation is that C_4H_8 is produced by the reaction between C_3H_6 and CH_4 on the ZSM-5 based catalyst, which may follow a similar pathway of the reaction between ethylene and methane, i.e., a methane molecule is incorporated into the light olefin and rejects H_2.[16,34] The effect of pressure on the formation of C_4H_8 and C_4H_{10}, however, differs from H_2 and C_2 products. The increment of C_4 products under CH_4 environment comparing with N_2 environment is enlarged at higher pressure. This phenomenon is consistent with the effect of pressure on the carbon number of liquid products. Another observation is that when methane is present, the amount of C_3H_8 is increased, which might be related to its H-rich environment that promotes the saturation of propylene.

3.2 Methane engagement verification

The direct evidence of methane participation into the upgrading reaction is observed in the NMR spectra when ^{13}C-labelled methane is employed in the reaction. Figure 3 displays the ^{13}C NMR spectra of the liquid products obtained when CH_4 and $^{13}CH_4$ are employed as the methane source to react with propylene under the facilitation of Ag-Ga/ZSM-5 catalyst. As is observed in the present work, a higher methane pressure enhances the participation of methane in the co-aromatization reaction. The partial pressure of $^{13}CH_4$ pressure is only 100 kPa in the reaction due to the availability of the isotopic labelled feedstock. Therefore, the extent of ^{13}C participation might be less significant compared with the aforementioned reactions. In the present work, the ^{13}C labeling study at a low pressure confirms the methane participation, which should be more significant at elevated methane pressures. The ^{13}C resonance present in the spectra can be divided into two groups. The peaks between 124-148 ppm are assigned to aromatic carbons, while those between 14-35 ppm are attributed to carbon sites of the alkyl side chains. The total peak area of

Pursuant to the DOE Public Access Plan, this document represents the authors' peer-reviewed, accepted manuscript.
The published version of the article is available from the relevant publisher.

the peaks at these two regions are increased to 2.2 and 2.5 times, respectively, where the areas of the solvent $CDCl_3$ peak are used as the internal reference, in the $^{13}CH_4$+propylene run compared to that from its non-isotopic labelled counterpart. During ^{13}C NMR measurement, in order to collect a large number of scans to improve the quality of the spectra, the recycle delay is not set long enough for all the excited ^{13}C nuclei to relax to ground state. As a result, the peak area may not be linearly proportional to the concentration of ^{13}C in the products. Nevertheless, the significantly escalated peak areas strongly indicate the ^{13}C enrichment under $^{13}CH_4$ environment, originating from the methane participation in the aromatization reaction. Based on the GC-MS analysis of the obtained liquid products, they are mainly composed of saturated aromatics with a molar percentage of unsaturated species including indene and 4-ethenyl-1,2-dimethylbenzene at 0.4%. The ^{13}C NMR signal of the carbon sites from the unsaturated bonds are not detected, which might be attributed to the low concentration of these sites. Combining with the product distribution obtained from GC-MS analysis and the ^{13}C chemical shift of variable carbons sites[35], the aromatic carbon NMR signals can be further categorized into four groups. The peaks at 137.3, 145.3 and 148.3 ppm are due to the phenyl carbon sites that are directly bonded to alkyl substituent groups. The signals between 132-136 ppm are attributed to the carbons sites shared by the two rings in indane and naphthalene. They could also be contributed by the naphthalene carbon sites bonded to alkyl substituent groups. The peaks that appear between 128-130 ppm are assigned to the phenyl ring carbon atoms that are on the ortho and meta positions of the alkyl substituent, while the others in the region of 124-127 ppm are due to the para carbon sites. Among these four groups, when $^{13}CH_4$ is employed, the peak intensities are increased to 2.0, 1.3, 2.0 and 2.6 times, respectively, compared with their non-isotopic counterparts, suggesting that the carbon atoms from methane tend to be incorporated into the phenyl para position while the carbon sites shared by the

Pursuant to the DOE Public Access Plan, this document represents the authors' peer-reviewed, accepted manuscript.
The published version of the article is available from the relevant publisher.

two indane and naphthalene rings are not favored. The enrichment phenomenon of ^{13}C at the alkyl carbon site region is also clearly observed on the spectra, suggesting that the carbon atoms from methane also get incorporated into the alkyl sites besides the phenyl ring carbon sites.

Besides $^{13}CH_4$, deuterium-enriched methane, i.e., CD_4, is also used as the methane source in the reaction in order to track the behavior of the methane hydrogen during the reaction. The ^1H and ^2D NMR spectra of the liquid product are acquired and compared with those of the non-isotopic enriched liquid products (Figure 4). On the ^1H NMR spectra, the peaks at 7.24 ppm are due to the $CHCl_3$ in the solvent, the intensities of which are similar in Figure 4a and 4b. The intensities of most other peaks, however, are suppressed significantly when CD_4 is present in the reaction. The peaks between 6.9~7.8 ppm are due to the H atoms on the phenyl rings, among which those around 7.48 and 7.84 ppm are assigned to the hydrogen sites on naphthalene rings. The signals between 2.0~2.8 ppm can be assigned to benzylic H sites. Those appearing at the region below 2 ppm are attributed to H sites of the alkyl groups that are not bonded to phenyl rings directly. The ratios between the peak areas with respect to that of $CHCl_3$ are shown in Table 2. The signals, especially those due to aromatics and benzylic H sites, are greatly reduced in the ^1H NMR spectrum collected from the isotopic labelled run, suggesting that a large portion of hydrogen in the liquid products come from methane. The peak at 5.3 ppm is assigned to the H from the unsaturated bonds. The peak intensity remains unchanged when the methane source is change from CH_4 to CD_4, indicating that these sites probably originate from the olefin feedstocks instead of methane. Compared with the peak area change observed in the ^{13}C NMR spectra, it is worth noting that the involvement of hydrogen is more profound than carbon from the methane molecules. It might be because compared with C atoms, there are more H atoms available in methane molecules, which may participate into the product molecules upon the cleavage of a single C-H bond. The

Pursuant to the DOE Public Access Plan, this document represents the authors' peer-reviewed, accepted manuscript.
The published version of the article is available from the relevant publisher.

incorporation of carbon atoms into the phenyl ring, however, involves the cleavage step of at least three C-H bonds, which may not be significant under the low reaction pressure. The change of peak areas also hints that methane hydrogens favor the aromatic and benzylic hydrogen sites over the alkyl group hydrogen sites. It is further confirmed by the ^{2}D NMR spectra (Figure 4c and 4d), where two strong NMR peaks are observed at the aromatic (7~8 ppm) and benzylic (2.5 ppm) site regions, along with a small peak attributed to alkyl D atoms in the spectrum where CD_4 is engaged as the methane source. The MS spectra of some aromatic products with relatively simple side chain structure including benzene, toluene, isopropylbenzene and 1,7-dimethylnaphthalene obtained under CH_4 and CD_4 conditions are displayed in Figure S1-S4. On the spectra of benzene, the peaks at m/z region of 76~79 are increased to 76~81. The increased m/z of 2 suggests that there are average two D atoms incorporated to each benzene molecule. This phenomenon is also observed on the spectra of toluene, which might suggest that the D incorporation into benzene and toluene is primarily during the phenyl ring formation step, compared with the methyl group incorporation step. On the MS spectrum of isopropylbenzene under CH_4 condition, there are two groups of peaks. The peaks at 120~121 are due to molecular ion peaks, while those around 105~106 are assigned to the piece after one methyl group is lost. When CD_4 is employed, the m/z value of molecular ion peaks are increased by 2 to 123, while the peaks around 105 are also increased by 2 to 108. This observation indicates that the loss of the first methyl group from isopropylbenzene, which not bonded to phenyl ring, does not significantly reduce the number of D atoms, i.e., the number of D atoms at this methyl site is small. This observation is consistent with the aforementioned phenomenon from NMR spectra that D is not rich in the alkyl groups that are not bonded to phenyl ring. Figure S4 shows the MS spectra of 1,7-dimethylnaphthalene. The molecular ion peak is increased by an m/z of 3 from 157 under CH_4 to 160 under CD_4. The peaks due to the moiety after

Pursuant to the DOE Public Access Plan, this document represents the authors' peer-reviewed, accepted manuscript.
The published version of the article is available from the relevant publisher.

412 the loss of methyl group, however, witnesses a m/z increase of 2 from 142 to 144, suggesting that
413 the average D atom number on the methyl species is 1, confirming that D atoms are rich in benzylic
414 sites.

415 In order to better understand the reaction mechanism, especially the significant ^{2}D-enrichment
416 at the benzylic site, styrene, which possesses an unsaturated -C=C- at the benzylic site, is also used
417 as the feedstock in the aromatization reaction. The liquid product is mainly composed of benzene,
418 toluene, ethylbenzene and naphthalene, based on the GC-MS analysis. The ^{1}H and ^{2}D NMR spectra
419 of the styrene upgrading liquid product are acquired and compared with those of the non-isotopic
420 enriched one (Figure 5) in order to understand the incorporation of the hydrogen atoms from
421 methane to the products. The peak area ratios to that of $CHCl_3$, the internal standard in the samples,
422 are tabulated in Table 2. It is clearly noticed that the enrichment of D, coming from methane, on
423 the benzylic sites in the product molecules becomes even more significant, suggesting that the
424 presence of unsaturated site could enhance the activation of methane. The drop of ^{1}H peak intensity
425 due to the alkyl hydrogen sites under CD_4 condition, however, is negligible, which is consistent
426 with the weak alkyl deuterium signal on the ^{2}D NMR spectrum. This observation may imply that
427 the hydrogen atoms that saturate styrene into ethylbenzene are not contributed by methane, but
428 primarily released during the aromatization of styrene into naphthalene.

429 To obtain a more comprehensive understanding of the evolution of methane during the reaction,
430 Diffuse Reflectance Infrared Fourier Transform (DRIFT) spectra are acquired to unveil the role
431 played by propylene as well as methane on the surface of the charged catalyst. As is displayed in
432 Figure 6, upon the adsorption of propylene, the IR pattern due to C-H stretch is plainly observed
433 at high wavenumber range of 2800-3000 cm^{-1}. It is clearly noticed that when CH_4 is present, the
434 peak intensity is higher than that of its N_2 counterpart. In this study, the DRIFT spectra are acquired

Pursuant to the DOE Public Access Plan, this document represents the authors' peer-reviewed, accepted manuscript.
The published version of the article is available from the relevant publisher.

on the catalyst surface without dilution to enhance the IR signal. Despite that the signal intensity change may not be proportional to the concentration of corresponding sites, the enhanced resonance indicates that some CH_4 is adsorbed on the surface, leading to the increased concentration of C-H bonds. IR vibration at this region, however, is not observed in the spectrum acquired under CH_4 environment without propylene introduction (not displayed in the figure), suggesting that the enhanced signal is related to the interaction between propylene and methane. In other words, propylene pre-adsorption might facilitate the methane adsorption on the catalyst surface. Besides, since propylene is only introduced to the reaction chamber where catalyst is charged at the beginning of the experiments, as the temperature gets higher, the peak intensity decays gradually due to desorption of surface species. At 100 and 200 ^{o}C, the enhanced peak intensity when methane is present is more significant, demonstrating that methane adsorption might be more favored and there might be stronger interaction existing between propylene and methane at these temperatures. However, this trend is reversed at 300 ^{o}C, which may be because that the product formed by the reaction taking place between the adsorbed propylene surface species and methane dissociates from the catalyst surface more easily compared to the thermal desorption of the adsorbed surface reactants without the engagement of methane. CD_4 is also employed to acquire the spectra, which are compared with the non-isotopic counterpart in order to study the evolution of methane on the catalyst surface. At 25 ^{o}C, the peak intensity is slightly lower under CD_4 condition, which can be attributed to the smaller amount of C-H bond. At 100 and 200 ^{o}C, however, the peak intensity is greatly increased compared with that under non-isotopic methane environment. Interestingly, the peak intensity is even higher than that observed at 25 ^{o}C. Considering the fact that propylene is introduced only once, before acquiring the spectra, and as a result, the C-H stretch signal should diminish gradually due to the thermal desorption of adsorbed

Pursuant to the DOE Public Access Plan, this document represents the authors' peer-reviewed, accepted manuscript.
The published version of the article is available from the relevant publisher.

surface species, the promoted signal intensity should be attributed to the introduced CD_4 between the acquisition of the spectra at 25 and 100 ^oC. In literature, it has been reported that upon the adsorption of CD_3CN on zeolites, a broad band at around 2900 cm^{-1} due to the interaction between CD_3CN and the hydroxyl groups from the zeolite surface is observed.[36,37] Based on this observation, the observed increased peak intensity might also be attributed to the interaction between adsorbed CD_4 and hydroxyl groups on the catalyst surface. Compare with the spectra collected under CD_4 condition without the introduction of propylene (Figure 6, green curves), where the peaks at 2800-3000 cm^{-1} region is absent, it can be almost certainly concluded that the increased peak intensity is due to the synergetic effect between propylene surface species, CD_4 and the catalyst. In order to further justify the methane activation compared with methane adsorption, the spectra at higher temperatures with CD_4 introduction are acquired. At 200 ^oC, two new peaks at 2754 and 2653 cm^{-1} are observed on the spectrum collected without propylene introduction, which become more significant when temperature is elevated to 300 ^oC. They can be assigned to the O-D stretch of the terminal silanol hydroxyl groups and bridging hydroxyl groups, respectively.[38] The formation of these O-D sites suggests the C-D bond cleavage in CD_4 molecules, implying the activation of methane on the surface of the catalyst. When propylene surface specie is present at 300 ^oC, i.e., under C_3H_6+CD_4 condition, the peak at 2754 cm^{-1} is shifted to 2746 cm^{-1}, strongly suggesting the interaction between propylene, methane and the hydroxyl groups of the catalyst.

The co-aromatization of methane and propylene over Ag-Ga/ZSM-5 catalyst is also investigated through employing DSC to study the heat effect of the reaction upon methane introduction. The heat flow when the mixture of propylene and methane is introduced at 400 ^oC (10~40 min) is displayed in Figure 7. For better comparison, the results collected from its N_2

Pursuant to the DOE Public Access Plan, this document represents the authors' peer-reviewed, accepted manuscript.
The published version of the article is available from the relevant publisher.

counterpart and the methane-alone run are also included. A stronger negative peak is clearly witnessed over propylene+methane run while that from its N_2 counterpart is a weak one, indicating more exothermic feature occurring from the interaction between methane and propylene molecules. When methane alone is introduced, a small negative peak is observed at ~10 min, which can be attributed to the exothermic feature occurring during adsorption of methane. The heat flow curve after that does not show strong endo- or exothermic effect, suggesting that the dramatically changed heat effect is due to the synergetic effect occurring between propylene and methane. Thermodynamic calculation is also carried out to explore the possible reason behind these phenomena. Due to the complexity of the products, it is difficult to include all the species in the calculation. Based on the analysis on the products obtained from the reaction between propylene and methane (Figure 1 and Table 1), the presence of methane increases the carbon number of the formed aromatics, for instance, more toluene over benzene. It also promotes the formation of C_3H_8 along with a small amount of C_4H_8. These key species may play an important role in the escalated exothermic feature of the reaction. Based on this assumption, they are considered in the thermodynamic calculation where the pressure of propylene and methane are set at 0.5 atm. At 400 ºC, the aromatization of propylene, i.e., $2C_3H_6 = C_6H_6 + 3H_2$, displays an enthalpy change of ΔH = -9.6 kcal/mol. When methane is present, resulting in an increased carbon number of aromatics and saturation of propylene, the reaction may be modified to $3C_3H_6 + CH_4 = C_7H_8+C_3H_8+3H_2$, with an enthalpy change of ΔH = -33.8 kcal/mol. When considering the enhanced formation of C_3H_8 and C_4H_8 under methane environment, the effect may be represented by $4C_3H_6 + 4CH_4 = C_4H_8 + 4C_3H_8$, where the enthalpy change is ΔH = -64.8 kcal/mol. The more negative enthalpy change of these reactions could contribute to the enhanced exothermic feature of the reaction in the presence of methane. Therefore, such exothermic heat effect of the

Pursuant to the DOE Public Access Plan, this document represents the authors' peer-reviewed, accepted manuscript.
The published version of the article is available from the relevant publisher.

propylene+methane run may provide another evidence of methane participation in the propylene aromatization reaction.

3.3 Correlation between catalyst properties and its performance

In order to identify the correlation between the physical properties of the catalyst and its catalytic performance, versatile characterization techniques including N_2 physisorption, XRD, TEM, DRIFTS, NH_3 TPD, TGA, and XPS have been employed in this study. The porous properties of various catalysts are analyzed through N_2 physisorption and the results are reported in Table 3. Compared to pure HZSM-5 support, Ag and Ga modified zeolite catalyst has increased total surface area and reduced pore volume. In addition, it is worth noting that upon metal loading the external surface area remains intact while the internal surface area is increased significantly, which is attributed to the additional surfaced area induced by metal particles. This phenomenon could benefit the aromatization reaction taking place within the zeolite pores[22] where active metal is well dispersed. After the reaction, the total surface area and pore volume are reduced, which might be due to the formation of coke and adsorption of product molecules.

The crystal phase evolution of the catalyst during the reaction is further investigated by resorting to XRD technique. Figure 8 shows the XRD patterns of HZSM-5 support as well as fresh and spent Ag-Ga/ZSM-5 catalyst. The peaks due to the oxide compounds of silver or gallium are not visible, which may be due to their excellent dispersion on the surface of the catalyst. After a closer comparison, it is also noticed that upon the introduction of Ag and Ga species into the HZSM-5 framework, the intensity of their diffraction peaks due to (011), (200) and (020) crystal planes are significantly enhanced in the fresh Ag-Ga/ZSM-5 catalyst. A plausible explanation is that the doped Ag and Ga species migrate into the HZSM-5 framework and enhance the crystalline of these planes. Over the reaction, such interaction is suppressed due to the evolution of the metal

Pursuant to the DOE Public Access Plan, this document represents the authors' peer-reviewed, accepted manuscript. The published version of the article is available from the relevant publisher.

species, leading to a reduced crystalline of these planes in the spent catalysts. It is noticed that the peak assigned to the (211) plane is small on the fresh Ag-Ga/ZSM-5, but turns stronger after the reaction, which might also be induced by the evolution of metal species during catalyst preparation and reaction process.

Besides XRD patterns released in Figure 8, the samples are further investigated by employing TEM technique. Figure 9 demonstrates the morphology of the Ag and Ga particles dispersed in fresh Ag-Ga/ZSM-5. Lots of small particles with an average size < 2 nm and a few with an average size of 5 nm are detected in Figure 9a and 9b. The elemental distribution on the surface of Ag-Ga/ZSM-5 is further studied by acquiring the EDX spectra of these small particles (Figure 9c) as well as the large ones (Figure 9d). It turns out that the large particles are Ag-rich while the small ones are formed by both Ag and Ga after careful analysis of the collected EDX spectra. The morphology of the spent catalyst after the reaction with propylene under N_2 and CH_4 environment is also investigated. The crystalline of the catalyst framework stays intact and the fringe of the zeolite structure is clearly observed (Figure 10a and 10e). Some large particles with a size of > 20 nm are observed on the catalyst. The EDX spectra of these large particles (Figure 10d and 10g) shows that the particles are composed of both Ag and Ga, while the EDX study of other areas on the framework (Figure 10c and 10h) reveals that the concentration of Ag and Ga is low. These observations suggest that the Ag-rich large particles and small particles composed of Ag and Ga in the fresh catalyst tend to form larger particles due to agglomeration during the aromatization reaction.

The surface acidity of the Ag-Ga/ZSM-5 catalyst as well as the HZSM-5 support is calibrated by choosing pyridine as the probe. Figure 11 shows the DRIFT spectra collected over HZSM-5 and Ag-Ga/ZSM-5 upon the adsorption of pyridine at room temperature. Despite that the Beer-

Pursuant to the DOE Public Access Plan, this document represents the authors' peer-reviewed, accepted manuscript.
The published version of the article is available from the relevant publisher.

Lambert law, where the absorbance is considered proportional to the concentration[39], may not necessarily hold for accurate quantification, the signals are presented in absorbance to better estimate the acid site concentration change upon metal loading. The peaks around 1440 cm^{-1} are assigned to Lewis acid sites[39,40], indicating the presence of Lewis acid sites on HZSM-5 and Ag-Ga/ZSM-5. The signal appearing at 1548 cm^{-1} on HZSM-5 spectrum is due to Brösted acid sites[41] upon pyridine adsorption, suggesting the presence of Brösted acid sites on HZSM-5. The other peaks identified in these spectra are also closely associated to the -OH group of the ZSM-5 framework. The peak at 1492 cm^{-1} on HZSM-5 spectrum is assigned to the 19a mode of pyridinium H-bonded with pyridine as well as the ZSM-5 framework. The signals at around 1600 cm^{-1} are assigned to the hydrogen-bonded pyridine. The peaks at 1642 cm^{-1} are due to the 8a and 8b mode of pyridinium H-bonded with pyridine and the ZSM-5 framework,[42] where the noted 8a, 8b, and 19a are the mode symbols.[43] These observations suggest that upon the loading of Ag and Ga species on the HZSM-5 framework, the original surface acidity of the ZSM-5 support is suppressed probably because of acidic sites occupation and the number of –OH groups is reduced as a result, while the Lewis acid sites are still present possibly the introduction of metal species on the surface of zeolite support.

The features of surface acidic sites of these catalysts are further analyzed using NH_3 TPD, the results of which are displayed in Figure 12 in order to compare the change upon metal modification and reaction. The low-temperature (LT) peak ranging from 200 to 400 ^oC might originate from the NH_3 molecules desorbed from the weak surface acidic sites and the high-temperature (HT) peak spanning from 400 to 600 ^oC is probably associated with NH_3 molecules desorbed from strong surface acidic sites.[44,45] The LT peak is observed over all the tested samples, implying the presence of weak acidic sites on the surface the catalysts. Upon Ag and Ga modification, the peak

Pursuant to the DOE Public Access Plan, this document represents the authors' peer-reviewed, accepted manuscript.
The published version of the article is available from the relevant publisher.

intensity at HT region is decreased, implying some strong acid sites are consumed. Despite the decreased intensity, the HT peaks are witnessed over all the catalyst samples, indicating that strong Brösted and Lewis acid sites are still available[22] on the catalyst surface, contributing to catalyzing methane and olefin aromatization reactions as suggested by the previous researches.[46–48] In addition, after quantification, the total acid amounts for HZSM-5, Ag-Ga/ZSM-5, spent Ag-Ga/ZSM-5 catalysts obtained under CH_4 and N_2 environment are determined to be 1,047, 526, 506 and 479 μmol NH_3/g_{cat}, respectively. Ag and Ga loadings into the HZSM-5 framework result in significant surface acidity reduction to almost half of its original value, which is consistent with what is observed in pyridine adsorption (Figure 11). Moreover, after the aromatization reaction the total acid amount available on catalyst surface is further reduced to certain degree, indicating that some acid sites might be further occupied probably by the formed coke. TGA analysis (Figure 13) shows that the coke deposit on the catalyst is 5.1% and 5.5% after the reaction under CH_4 and N_2, respectively, when only the second major weight loss is taken into consideration because the first one is mainly due to the desorption of the surface species formed during aromatization reaction. The suppressed coke deposit under CH_4 environment could be related to the larger number of total acid sites remaining upon the reaction, which might play a role on the improved aromatization performance under CH_4 environment.

In order to get a better understanding of how each element contained in the Ag-Ga/ZSM-5 gets distributed on the catalyst surface and their corresponding oxidation state, XPS is employed to conduct specific scans at O 1s, Ag 3d, Ga 2p and C 1s regions, respectively. The results are disseminated in Figure 14. Figure 14a shows the XPS spectra acquired at Ag 3d region. The binding energies due to 3d orbitals are shifted to higher value during the reaction, indicating a partial reduction of silver species. Gabrienko et al[24] studied the function of silver species on

Pursuant to the DOE Public Access Plan, this document represents the authors' peer-reviewed, accepted manuscript. The published version of the article is available from the relevant publisher.

Ag/ZSM-5 catalyst in methane activation and the reaction intermediates. It was observed methane is converted to O-CH_3 and Ag-H upon the C-H bond cleavage, followed by the formation of ethylene, which was absorbed by silver cations. The participation of silver cations as catalytic active site in the activation process of both methane and -C=C- bond may contribute to the observed reduction. After the reaction the surface concentration of Ag gets decreased probably due to its diffusion from the surface towards the inner pores of the zeolite support, which is consistent with the observation on Ag-Ga modified ZSM-5 catalyst over olefin upgrading under CH_4 environment.[49] The concentration of silver species, however, is higher under CH_4 environment. The spectra at the O 1s region are displayed in Figure 14b. There are two O sites observed in the fresh catalyst spectrum. The one at 532.1 eV might be contributed by the Ag_2O and Ga_2O_3 species[50,51], while the one at 532.9 eV may be assigned to the SiOH groups on the catalyst surface.[52] The O surface concentration due to the oxide species is reduced after aromatization reaction which is consistent with the hypothesis that some silver oxide compound migrates to the inner pores of the catalyst. Figure 14c demonstrates the XPS spectra collected at the Ga 2p region. The reduced signal intensity upon the reaction indicates that the gallium oxide species might also migrate into the inner pores of the catalyst during the reaction. Based on the above observation, it can be concluded that during reaction silver species as well as the gallium oxide tend to diffuse into the inner pores of the catalyst where is the place aromatization reaction would probably prefer to talk place according to the previous study[22]. More silver oxide species remains on the surface of the catalyst under CH_4 environment, which might be closely associated with the better catalytic performance when CH_4 is present. The increased C 1s signals collected from the spent catalysts (Figure 14d) provide another evidence of coke formation during aromatization reaction when that from the fresh sample is referred in the same figure.

Pursuant to the DOE Public Access Plan, this document represents the authors' peer-reviewed, accepted manuscript.
The published version of the article is available from the relevant publisher.

4 Conclusions

The present work demonstrates the technical feasibility of simultaneous aromatization of propylene and methane over Ag and Ga modified HZSM-5 catalyst at a low temperature of 400 ºC, which is close to the temperature of petroleum refining processes. Methane is activated and incorporated into the formed aromatics leading to increased carbon number of both gas and liquid products, along with more exothermic reaction feature. The participation of methane is directly evidenced by ^{1}H, ^{2}D and ^{13}C NMR study of the liquid products. The hydrogen from methane tend to occupy the benzylic sites as well as aromatic hydrogen sites in the product molecules. The interaction between propylene and methane on the catalyst surface can be observed by FTIR starting from 100 ºC. The C-H bond cleavage of methane is detected at 200 ºC, which becomes more significant at 300 ºC, leading to a clear interaction with propylene surface species. The excellent catalytic performance of Ag-Ga/ZSM-5 might be because of the better dispersion of Ag and Ga on the ZSM-5 surface and moderate amount of strong Brösted and Lewis surface acid sites which may also result in coke formation. Therefore, tuning the surface acidity of charged catalyst for balancing its aromatization performance and coke resistance as well as metal agglomeration prevention for stability enhancement would be a critical future work.

Acknowledgements

We gratefully acknowledge the financial supports from Meg Energy Corp. and Alberta Innovates - Energy and Environment Solutions (AI-EES, 2142).

Pursuant to the DOE Public Access Plan, this document represents the authors' peer-reviewed, accepted manuscript. The published version of the article is available from the relevant publisher.

642

643 **References**

644 [1] J.H. Lunsford, The Catalytic Oxidative Coupling of Methane, Angew. Chemie Int. Ed. 34
645 (1995) 970–980. doi:10.1002/anie.199509701.

646 [2] Y. Amenomiya, V.I. Birss, M. Goledzinowski, J. Galuszka, A.R. Sanger, Conversion of
647 methane by oxidative coupling, Catal. Rev. 32 (1990) 163–227.
648 doi:10.1080/01614949009351351.

649 [3] U. Zavyalova, M. Holena, R. Schlögl, M. Baerns, Statistical analysis of past catalytic data
650 on oxidative methane coupling for new insights into the composition of high-performance
651 catalysts, ChemCatChem. 3 (2011) 1935–1947. doi:10.1002/cctc.201100186.

652 [4] C. Li, C. Dinoi, Y. Coppel, M. Etienne, CH Bond Activation of Methane by a Transient η 2
653 -Cyclopropene/Metallabicyclobutane Complex of Niobium, J. Am. Chem. Soc. 137 (2015)
654 12450–12453. doi:10.1021/jacs.5b07859.

655 [5] V.R. Choudhary, K.C. Mondal, S.A.R. Mulla, Simultaneous conversion of methane and
656 methanol into gasoline over bifunctional Ga-, Zn-, In-, and/or Mo-modified ZSM-5 zeolites,
657 Angew. Chemie Int. Ed. 117 (2005) 4455–4459. doi:10.1002/anie.200500694.

658 [6] Y. Cui, Y. Xu, J. Lu, Y. Suzuki, Z.G. Zhang, The effect of zeolite particle size on the activity
659 of Mo/HZSM-5 in non-oxidative methane dehydroaromatization, Appl. Catal. A Gen. 393
660 (2011) 348–358. doi:10.1016/j.apcata.2010.12.017.

661 [7] Y. Xu, X. Bao, L. Lin, Direct conversion of methane under nonoxidative conditions, J. Catal.
662 216 (2003) 386–395. doi:10.1016/S0021-9517(02)00124-0.

663 [8] V.T.T. Ha, A. Sarioglan, A. Erdem-Senatalar, Y. Ben Taarit, An EPR and NMR study on
664 Mo/HZSM-5 catalysts for the aromatization of methane: Investigation of the location of the

Pursuant to the DOE Public Access Plan, this document represents the authors' peer-reviewed, accepted manuscript.
The published version of the article is available from the relevant publisher.

pentavalent molybdenum, J. Mol. Catal. A Chem. 378 (2013) 279–284. doi:10.1016/j.molcata.2013.06.020.

[9] X. Guo, G. Fang, G. Li, H. Ma, H. Fan, L. Yu, C. Ma, X. Wu, D. Deng, M. Wei, D. Tan, R. Si, S. Zhang, J. Li, L. Sun, Z. Tang, X. Pan, X. Bao, Direct, nonoxidative conversion of methane to ethylene, aromatics, and hydrogen., Science. 344 (2014) 616–619. doi:10.1126/science.1253150.

[10] T. V. Choudhary, E. Aksoylu, D. Wayne Goodman, Nonoxidative Activation of Methane, Catal. Rev. 45 (2003) 151–203. doi:10.1081/CR-120017010.

[11] P. Tang, Q. Zhu, Z. Wu, D. Ma, Methane activation: the past and future, Energy Environ. Sci. 7 (2014) 2580–2591. doi:10.1039/C4EE00604F.

[12] J. Xue, Y. Chen, Y. Wei, A. Feldhoff, H. Wang, J. Caro, Gas to Liquids: Natural Gas Conversion to Aromatic Fuels and Chemicals in a Hydrogen-Permeable Ceramic Hollow Fiber Membrane Reactor, ACS Catal. 6 (2016) 2448–2451. doi:10.1021/acscatal.6b00004.

[13] V. Abdelsayed, D. Shekhawat, M.W. Smith, Effect of Fe and Zn promoters on Mo/HZSM-5 catalyst for methane dehydroaromatization, Fuel. 139 (2015) 401–410. doi:10.1016/j.fuel.2014.08.064.

[14] J.J. Spivey, G. Hutchings, Catalytic aromatization of methane, Chem. Soc. Rev. 43 (2014) 792–803. doi:10.1039/c3cs60259a.

[15] V.R. Choudhary, A.K. Kinage, T. V. Choudhary, Low-temperature nonoxidative activation of methane over H-galloaluminosilicate (MFI) zeolite, Science. 275 (1997) 1286–1288. doi:10.1126/science.275.5304.1286.

[16] T. Baba, H. Sawada, Conversion of methane into higher hydrocarbons in the presence of ethylene over H-ZSM-5 loaded with silver cations, Phys. Chem. Chem. Phys. 4 (2002)

Pursuant to the DOE Public Access Plan, this document represents the authors' peer-reviewed, accepted manuscript. The published version of the article is available from the relevant publisher.

688 3919–3923. doi:10.1039/b200615b.
689 [17] T. Baba, Y. Abe, Metal cation-acidic proton bifunctional catalyst for methane activation:
690 Conversion of 13CH4 in the presence of ethylene over metal cations-loaded H-ZSM-5, Appl.
691 Catal. A Gen. 250 (2003) 265–270. doi:10.1016/S0926-860X(03)00321-1.
692 [18] O.A. Anunziata, G. V Gonzalez, L.B. Pierella, Catalytic activation of methane using n-
693 pentane as co-reactant over Zn/H-ZSM-11 zeolite, Catal. Letters. 87 (2003) 167–171.
694 [19] O.A. Anunziata, G.G. Mercado, L.B. Pierella, Improvement of methane activation using n-
695 hexane as co-reactant over Zn/HZSM-11 zeolite, Catal. Commun. 5 (2004) 401–405.
696 doi:10.1016/j.catcom.2004.04.008.
697 [20] P. He, W. Shan, Y. Xiao, H. Song, Performance of Zn/ZSM-5 for in Situ Catalytic Upgrading
698 of Pyrolysis Bio-oil by Methane, Top. Catal. 59 (2016) 86–93. doi:10.1007/s11244-015-
699 0508-4.
700 [21] M. V. Luzgin, V.A. Rogov, S.S. Arzumanov, A. V. Toktarev, A.G. Stepanov, V.N. Parmon,
701 Understanding methane aromatization on a Zn-modified high-silica zeolite, Angew. Chemie
702 Int. Ed. 47 (2008) 4559–4562. doi:10.1002/anie.200800317.
703 [22] A. Wang, P. He, M. Yung, H. Zeng, H. Qian, H. Song, Catalytic co-aromatization of ethanol
704 and methane, Appl. Catal. B Environ. 198 (2016) 480–492.
705 doi:10.1016/j.apcatb.2016.06.013.
706 [23] M. V. Luzgin, V.A. Rogov, S.S. Arzumanov, A. V. Toktarev, A.G. Stepanov, V.N. Parmon,
707 Methane aromatization on Zn-modified zeolite in the presence of a co-reactant higher
708 alkane: How does it occur?, Catal. Today. 144 (2009) 265–272.
709 doi:10.1016/j.cattod.2008.08.043.
710 [24] A.A. Gabrienko, S.S. Arzumanov, I.B. Moroz, A. V. Toktarev, W. Wang, A.G. Stepanov,

Pursuant to the DOE Public Access Plan, this document represents the authors' peer-reviewed, accepted manuscript.
The published version of the article is available from the relevant publisher.

711 Methane activation and transformation on Ag/H-ZSM-5 zeolite studied with solid-state
712 NMR, J. Phys. Chem. C. 117 (2013) 7690–7702. doi:10.1021/jp4006795.
713 [25] Y.G. Kolyagin, I.I. Ivanova, V. V. Ordomsky, A. Gedeon, Y.A. Pirogov, Methane activation
714 over Zn-modified MFI zeolite: NMR evidence for Zn-methyl surface species formation, J.
715 Phys. Chem. C. 112 (2008) 20065–20069. doi:10.1021/jp8067766.
716 [26] J. Xu, A. Zheng, X. Wang, G. Qi, J. Su, J. Du, Z. Gan, J. Wu, W. Wang, F. Deng, Room
717 temperature activation of methane over Zn modified H-ZSM-5 zeolites: Insight from solid-
718 state NMR and theoretical calculations, Chem. Sci. 3 (2012) 2932–2940.
719 doi:10.1039/c2sc20434g.
720 [27] C. Mukarakate, M.J. Watson, J. ten Dam, X. Baucherel, S. Budhi, M.M. Yung, H. Ben, K.
721 Iisa, R.M. Baldwin, M.R. Nimlos, Upgrading biomass pyrolysis vapors over β-zeolites: role
722 of silica-to-alumina ratio, Green Chem. 16 (2014) 4891–4905. doi:10.1039/C4GC01425A.
723 [28] C.D. Baertsch, H.H. Funke, J.L. Falconer, R.D. Noble, Permeation of Aromatic
724 Hydrocarbon Vapors through Silicalite−Zeolite Membranes, J. Phys. Chem. 100 (1996)
725 7676–7679. doi:10.1021/jp960226h.
726 [29] A. Primo, H. Garcia, Zeolites as catalysts in oil refining., Chem. Soc. Rev. 43 (2014) 7548–
727 7561. doi:10.1039/c3cs60394f.
728 [30] P. He, Y. Xiao, Y. Tang, J. Zhang, H. Song, Simultaneous Low-Cost Carbon Sources and
729 CO 2 Valorizations through Catalytic Gasification, Energy & Fuels. 29 (2015) 7497–7507.
730 doi:10.1021/acs.energyfuels.5b01712.
731 [31] W. Ding, G.D. Meitzner, E. Iglesia, The Effects of Silanation of External Acid Sites on the
732 Structure and Catalytic Behavior of Mo/H–ZSM5, J. Catal. 206 (2002) 14–22.
733 doi:10.1006/jcat.2001.3457.

Pursuant to the DOE Public Access Plan, this document represents the authors' peer-reviewed, accepted manuscript.
The published version of the article is available from the relevant publisher.

734 [32] P. Bijani, M. Sohrabi, S. Sahebdelfar, Thermodynamic Analysis of Nonoxidative
735 Dehydroaromatization of Methane, Chem. Eng. Technol. 35 (2012) 1825–1832.
736 doi:10.1002/ceat.201100436.
737 [33] M.-F. Hsieh, Y. Zhou, H. Thirumalai, L.C. Grabow, J.D. Rimer, Silver-Promoted
738 Dehydroaromatization of Ethylene over ZSM-5 Catalysts, ChemCatChem. (2017) 1–9.
739 doi:10.1002/cctc.201700192.
740 [34] T. Baba, Y. Iwase, K. Inazu, D. Masih, A. Matsumoto, Catalytic properties of silver-
741 exchanged zeolites for propene production by conversion of methane in the presence of
742 ethene, Microporous Mesoporous Mater. 101 (2007) 142–147.
743 doi:10.1016/j.micromeso.2006.11.004.
744 [35] E. Pretsch, P. Buhlmann, M. Badertscher, Structure Determination of Organic Compounds,
745 Springer Berlin Heidelberg, 2009. doi:10.1007/978-3-540-93810-1.
746 [36] J. Chen, J.M. Thomas, G. Sankar, IR spectroscopic study of CD3CN adsorbed on ALPO-18
747 molecular sieve and the solid acid catalysts SAPO-18 and MeAPO-18, J. Chem. Soc.
748 Faraday Trans. 90 (1994) 3455. doi:10.1039/ft9949003455.
749 [37] J. Jänchen, J.H.M.C. Wolput, L.J.M. Ven, J.W. Haan, R. a. Santen, J.H.M.C. van Wolput,
750 L.J.M. van de Ven, J.W. de Haan, R.A. van Santen, FTIR spectroscopic and1 H MAS NMR
751 studies of the influence of lattice chemistry and structure on Brønsted acidity in zeolites,
752 Catal. Letters. 39 (1996) 147–152. doi:10.1007/BF00805574.
753 [38] J.N. Kondo, K. Domen, IR observation of adsorption and reactions of olefins on H-form
754 zeolites, J. Mol. Catal. A Chem. 199 (2003) 27–38. doi:10.1016/S1381-1169(03)00015-3.
755 [39] D. Yi, H. Huang, X. Meng, L. Shi, Adsorption-desorption behavior and mechanism of
756 dimethyl disulfide in liquid hydrocarbon streams on modified Y zeolites, Appl. Catal. B

Pursuant to the DOE Public Access Plan, this document represents the authors' peer-reviewed, accepted manuscript.
The published version of the article is available from the relevant publisher.

Environ. 148–149 (2014) 377–386. doi:10.1016/j.apcatb.2013.11.027.

[40] S.M.T. Almutairi, B. Mezari, E.A. Pidko, P.C.M.M. Magusin, E.J.M. Hensen, Influence of steaming on the acidity and the methanol conversion reaction of HZSM-5 zeolite, J. Catal. 307 (2013) 194–203. doi:10.1016/j.jcat.2013.07.021.

[41] W. Xu, S.J. Miller, P.K. Agrawal, C.W. Jones, Zeolite topology effects in the alkylation of phenol with propylene, Appl. Catal. A Gen. 459 (2013) 114–120. doi:10.1016/j.apcata.2013.03.019.

[42] R. Buzzoni, S. Bordiga, G. Ricchiardi, C. Lamberti, A. Zecchina, G. Bellussi, Interaction of Pyridine with Acidic (H-ZSM5, H-β, H-MORD Zeolites) and Superacidic (H-Nafion Membrane) Systems: An IR Investigation, Langmuir. 12 (1996) 930–940. doi:10.1021/la950571i.

[43] V.P. Glazunov, S.E. Odinokov, Infrared spectra of pyridinium salts in solution-I. The region of middle frequencies, Spectrochim. Acta Part A Mol. Spectrosc. 38 (1982) 399–408. doi:10.1016/0584-8539(82)80014-7.

[44] F. Lónyi, J. Valyon, On the interpretation of the NH3-TPD patterns of H-ZSM-5 and H-mordenite, Microporous Mesoporous Mater. 47 (2001) 293–301. doi:10.1016/S1387-1811(01)00389-4.

[45] H.G. Karge, Comparative Measurements on Acidity of Zeolites, in: Stud. Surf. Sci. Catal., 1991: pp. 133–156. doi:10.1016/S0167-2991(08)62903-1.

[46] Y. Xu, S. Liu, X. Guo, L. Wang, M. Xie, Methane activation without using oxidants over Mo/HZSM-5 zeolite catalysts, Catal. Letters. 30 (1995) 135–149. doi:10.1007/BF00813680.

[47] Y. Shu, Y. Xu, S. Wong, L. Wang, X. Guo, Promotional Effect of Ru on the Dehydrogenation and Aromatization of Methane in the Absence of Oxygen over Mo / HZSM-5 Catalysts, J.

Pursuant to the DOE Public Access Plan, this document represents the authors' peer-reviewed, accepted manuscript. The published version of the article is available from the relevant publisher.

Catal. 19 (1997) 11–19. doi:http://dx.doi.org/10.1006/jcat.1997.1726.

[48] K.S. Wong, J.W. Thybaut, E. Tangstad, M.W. Stöcker, G.B. Marin, Methane aromatisation based upon elementary steps: Kinetic and catalyst descriptors, Microporous Mesoporous Mater. 164 (2012) 302–312. doi:10.1016/j.micromeso.2012.07.002.

[49] P. He, Y. Lou, H. Song, Olefin upgrading under methane environment over Ag-Ga/ZSM-5 catalyst, Fuel. 182 (2016) 577–587. doi:10.1016/j.fuel.2016.05.126.

[50] C. Tang, W. Sun, W. Yan, Green and facile fabrication of silver nanoparticles loaded activated carbon fibers with long-lasting antibacterial activity, RSC Adv. 4 (2014) 523–530. doi:10.1039/C3RA44799E.

[51] D.Y. Guo, Z.P. Wu, Y.H. An, P.G. Li, P.C. Wang, X.L. Chu, X.C. Guo, Y.S. Zhi, M. Lei, L.H. Li, W.H. Tang, Unipolar resistive switching behavior of amorphous gallium oxide thin films for nonvolatile memory applications, Appl. Phys. Lett. 106 (2015) 2–7. doi:10.1063/1.4907174.

[52] K.A. Almeida, R. Landers, D. Cardoso, Properties of faujasite zeolites containing methyl-substituted ammonium cations, J. Catal. 294 (2012) 151–160. doi:10.1016/j.jcat.2012.07.017.

Pursuant to the DOE Public Access Plan, this document represents the authors' peer-reviewed, accepted manuscript. The published version of the article is available from the relevant publisher.

803

804 **Figure Captions**

805 **Figure 1.** The component distribution of the products obtained from the reaction between
806 propylene and methane at 1.0 (a), 3.0 (b), 5.0 (c) and 7.0 (d) MPa and 400 ^{o}C for 1 h

807 **Figure 2.** The ratio between toluene and benzene (a) and the average carbon number (b) of the
808 products obtained from the reaction between propylene and methane at variable pressures

809 **Figure 3.** The ^{13}C NMR spectra of the liquid products collected from the reaction between
810 propylene and CH_4/$^{13}CH_4$

811 **Figure 4.** The ^{1}H NMR spectra (a and b) and ^{2}D NMR spectra (c and d) of the liquid products
812 collected from the reaction between propylene and CH_4/CD_4

813 **Figure 5.** The ^{1}H NMR spectra (a and b) and ^{2}D NMR spectra (c and d) of the liquid products
814 collected from the reaction between styrene and CH_4/CD_4

815 **Figure 6.** DRIFT spectra acquired upon propylene adsorption over Ag-Ga/ZSM-5 under N_2, CH_4
816 and CD_4 atmosphere at various temperatures. Spectra acquired under CD_4 without propylene
817 introduction are displayed by the green curves

818 **Figure 7.** The DSC profiles collected during the reaction of styrene over Ag-Ga/ZSM-5 under
819 various environments and methane-alone run at 400 ^{o}C and 1 atm

820 **Figure 8.** XRD patterns of HZSM-5 and Ag-Ga/ZSM-5 before and after reaction with propylene
821 under various environments at 7.0 MPa and 400 ^{o}C for 1h

822 **Figure 9.** TEM images of fresh Ag-Ga/ZSM-5 in Bright Field (a) and High Angle Annual Dark
823 Field (b), and the EDX spectra (c and d) acquired at the corresponding areas in (b)

824 **Figure 10.** TEM images of spent Ag-Ga/ZSM-5 catalyst collected under CH_4 and N_2 environments
825 at 7.0 MPa in Bright Field (a and e) and High Angle Annual Dark Field (b and f), and the EDX
826 spectra (c, d, g and h) acquired at the corresponding areas in (b and f)

Pursuant to the DOE Public Access Plan, this document represents the authors' peer-reviewed, accepted manuscript.
The published version of the article is available from the relevant publisher.

827 **Figure 11.** The DRIFT spectra collected over HZSM-5 and Ag-Ga/ZSM-5 upon pyridine
828 adsorption at room temperature

829 **Figure 12.** The NH_3-TPD profiles collected over different catalysts

830 **Figure 13.** TGA profiles collected over spent Ag-Ga/ZSM-5 after reaction with propylene at 7.0
831 MPa and 400 ^oC for 1 h under CH_4 and N_2

832 **Figure 14.** XPS spectra of Ag-Ga/ZSM-5 before and after reaction with propylene at 7.0 MPa and
833 400 ^oC for 1 h under different environments at Ag 3d (a), O 1s (b), Ga $2p_{3/2}$ (c) and C 1s (d) regions

834

835 **Tables**

836 **Table 1.** The gas phase products and methane conversion after the reaction between C_3H_6 and CH_4
837 over Ag-Ga/ZSM-5 catalyst

838 **Table 2.** ^1H NMR peak area ratio with respect to $CHCl_3$ of the aromatization products of propylene
839 and styrene under CH_4 and CD_4 environment

840 **Table 3.** The porous properties of various catalysts

Pursuant to the DOE Public Access Plan, this document represents the authors' peer-reviewed, accepted manuscript.
The published version of the article is available from the relevant publisher.

Table 1. The gas phase products and methane conversion after the reaction between C_3H_6 and CH_4 over Ag-Ga/ZSM-5 catalyst

Pressure/MPa	1.0		3.0		5.0		7.0	
Gas phase	N_2	CH_4	N_2	CH_4	N_2	CH_4	N_2	CH_4
H_2	1.8	2.6	0.8	1.1	0	0	0	0
Methane	0.5	0.9[a]	0	3.9[a]	0	13.0[a]	0	13.9[a]
C_2H_4	0	0.002	0.01	0.01	0	0.01	0	0
C_2H_6	0.28	1.2	0.05	0.55	0	0	0	0
C_3H_6	5.9[a]	5.9[a]	5.9[a]	6.1[a]	5.9[a]	5.9[a]	5.9[a]	6.0[a]
C_3H_8	2.3	3.1	2.2	2.7	2.1	2.4	2.0	1.9
C_4H_8	0	0.21	0	0.33	0	0.35	0	0.41
C_4H_{10}	0.19	0.20	0.28	0.35	0.25	0.34	0.30	0.39
CH_4 conversion/%	-	1.8	-	2.3	-	4.7	-	3.8

a) converted CH_4 and C_3H_6; unit of data in this table is in mmol

Pursuant to the DOE Public Access Plan, this document represents the authors' peer-reviewed, accepted manuscript. The published version of the article is available from the relevant publisher.

Table 2. ^{1}H NMR peak area ratio with respect to $CHCl_3$ of the aromatization products of propylene and styrene under CH_4 and CD_4 environment

H/D sites	Propylene			Styrene		
	CH_4	CD_4	Decrease/%	CH_4	CD_4	Decrease/%
Aromatics	23.0	9.2	60	19.7	5.3	73
Benzylic	18.1	6.7	63	2.9	0.51	83
Alkyl	11.4	7.1	38	4.4	4.3	2

Pursuant to the DOE Public Access Plan, this document represents the authors' peer-reviewed, accepted manuscript. The published version of the article is available from the relevant publisher.

Table 3. The porous properties of various catalysts

Samples	BET Surface Area (m^2/g)			Porous Volume (cm^3/g)		
	External	Microporous	Total	Microporous	Mesoporous	Total
HZSM-5	109	292	401	0.149	0.142	0.291
Ag-Ga/ZSM-5	108	346	454	0.142	0.138	0.280
Ag-Ga/ZSM-5 CH_4	86	241	327	0.123	0.112	0.235
Ag-Ga/ZSM-5 N_2	83	256	339	0.131	0.120	0.251

Pursuant to the DOE Public Access Plan, this document represents the authors' peer-reviewed, accepted manuscript.
The published version of the article is available from the relevant publisher.

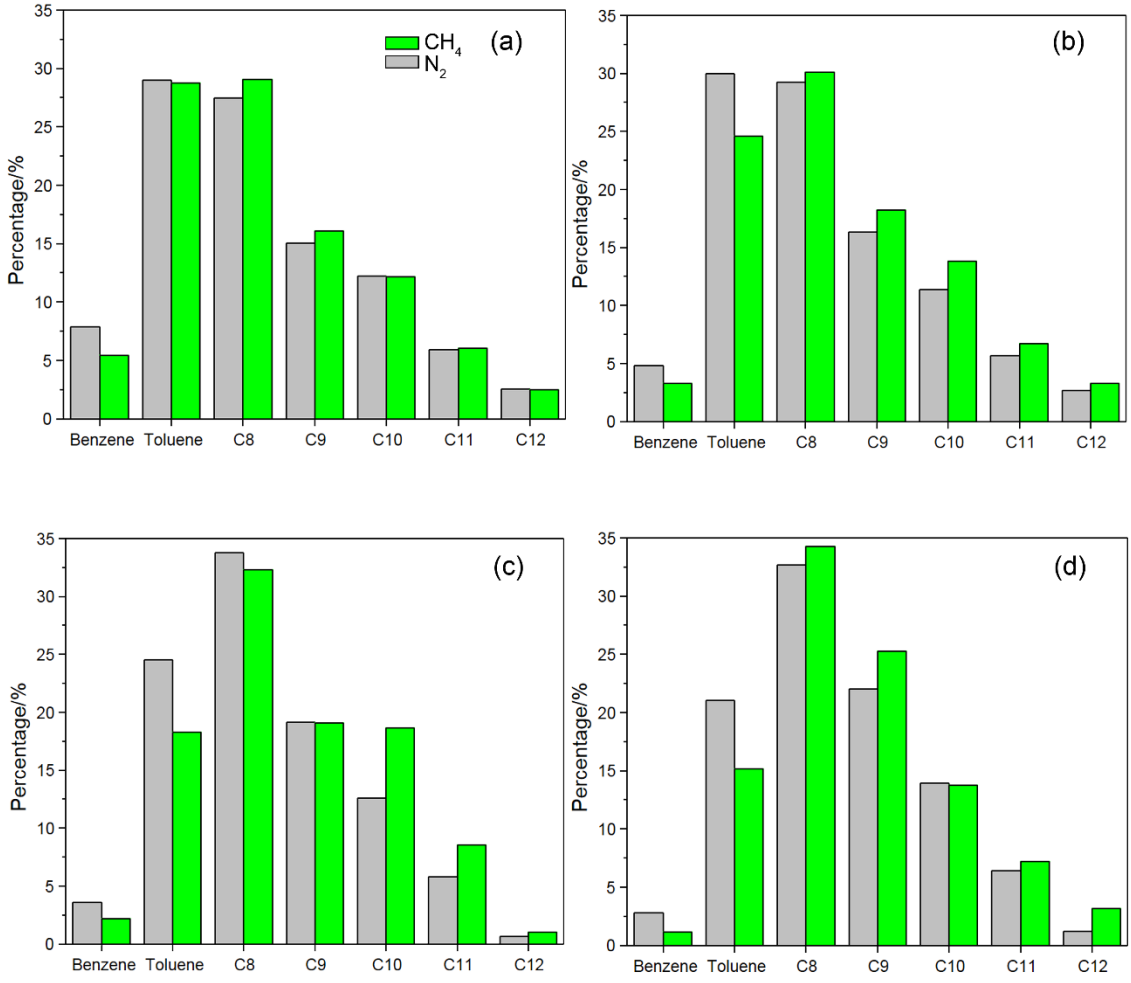

Figure 1. The component distribution of the products obtained from the reaction between propylene and methane at 1.0 (a), 3.0 (b), 5.0 (c) and 7.0 (d) MPa and 400 ºC for 1 h

Pursuant to the DOE Public Access Plan, this document represents the authors' peer-reviewed, accepted manuscript. The published version of the article is available from the relevant publisher.

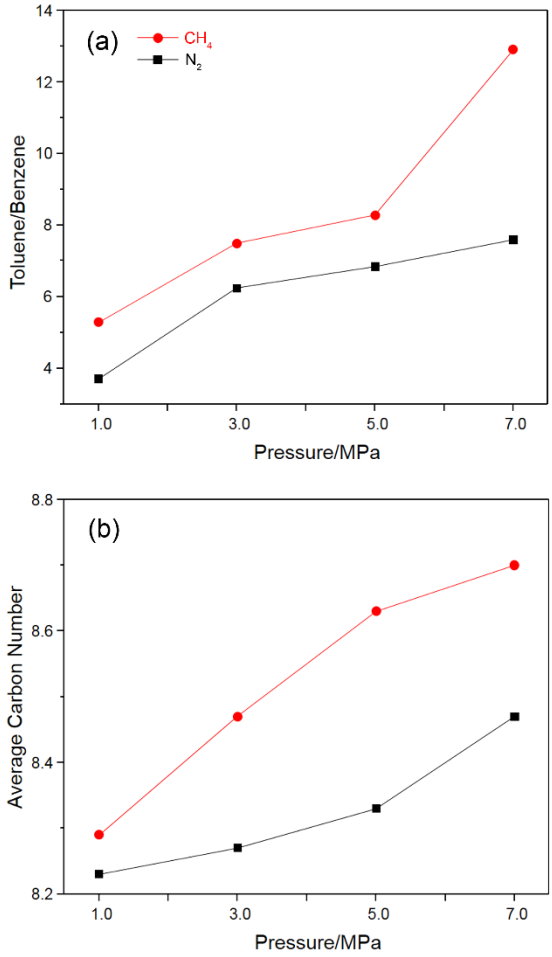

Figure 2. The ratio between toluene and benzene (a) and the average carbon number (b) of the products obtained from the reaction between propylene and methane at 1.0, 3.0, 5.0 and 7.0 MPa and 400 ºC for 1 h

Pursuant to the DOE Public Access Plan, this document represents the authors' peer-reviewed, accepted manuscript. The published version of the article is available from the relevant publisher.

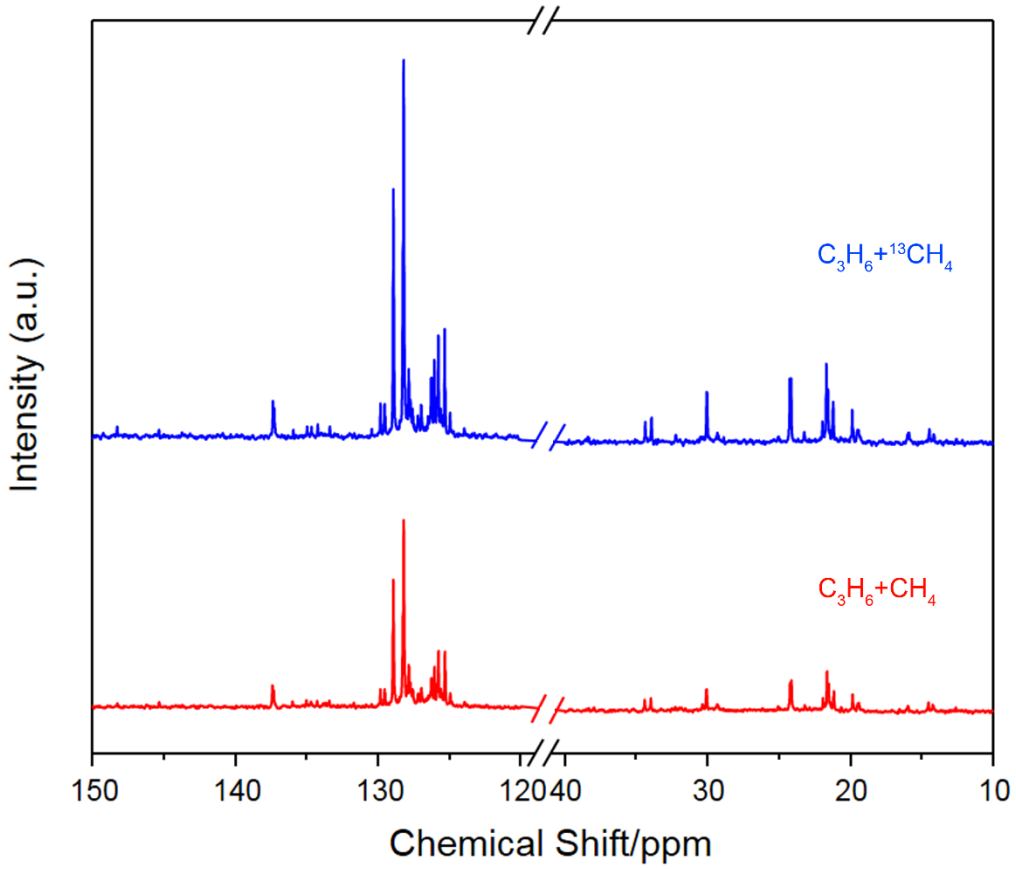

Figure 3. The ^{13}C NMR spectra of the liquid products collected from the reaction between propylene and $CH_4/^{13}CH_4$ at 0.3 MPa and 400 ^oC for 1 h

Pursuant to the DOE Public Access Plan, this document represents the authors' peer-reviewed, accepted manuscript. The published version of the article is available from the relevant publisher.

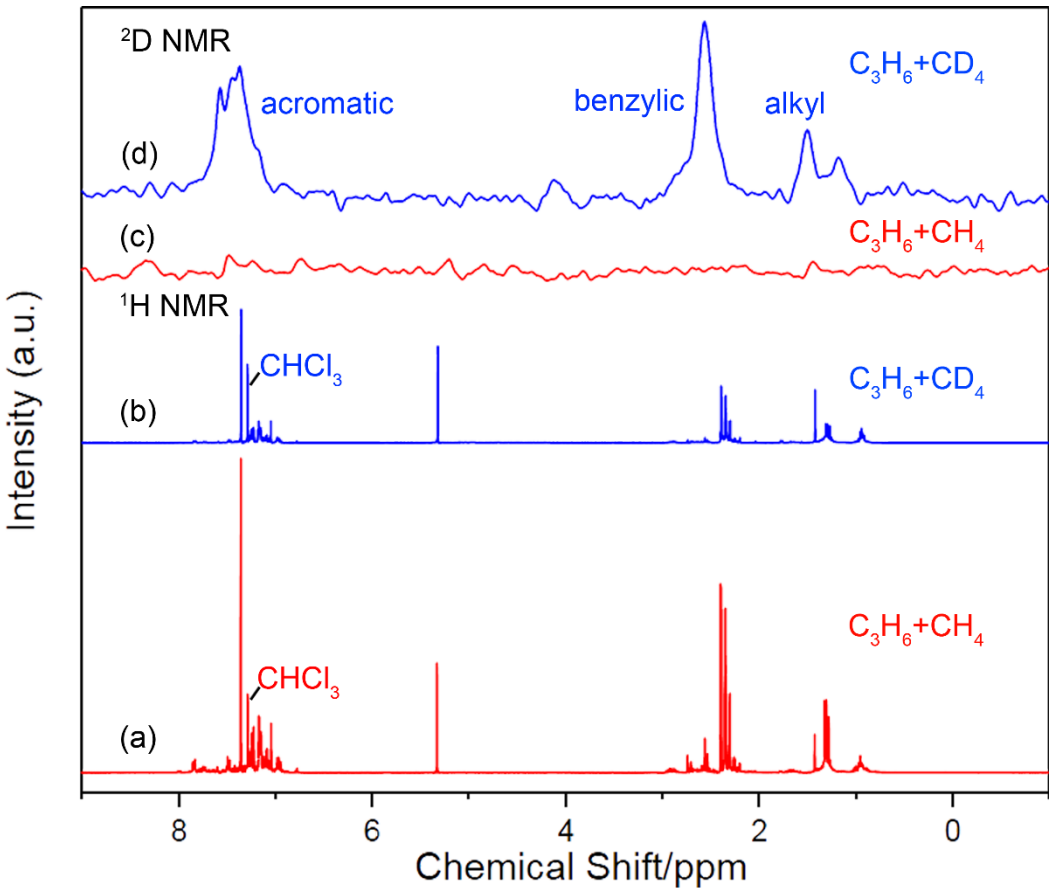

Figure 4. The ^{1}H NMR spectra (a and b) and ^{2}D NMR spectra (c and d) of the liquid products collected from the reaction between propylene and CH_4/CD_4 at 0.3 MPa and 400 ^{o}C for 1 h

Pursuant to the DOE Public Access Plan, this document represents the authors' peer-reviewed, accepted manuscript.
The published version of the article is available from the relevant publisher.

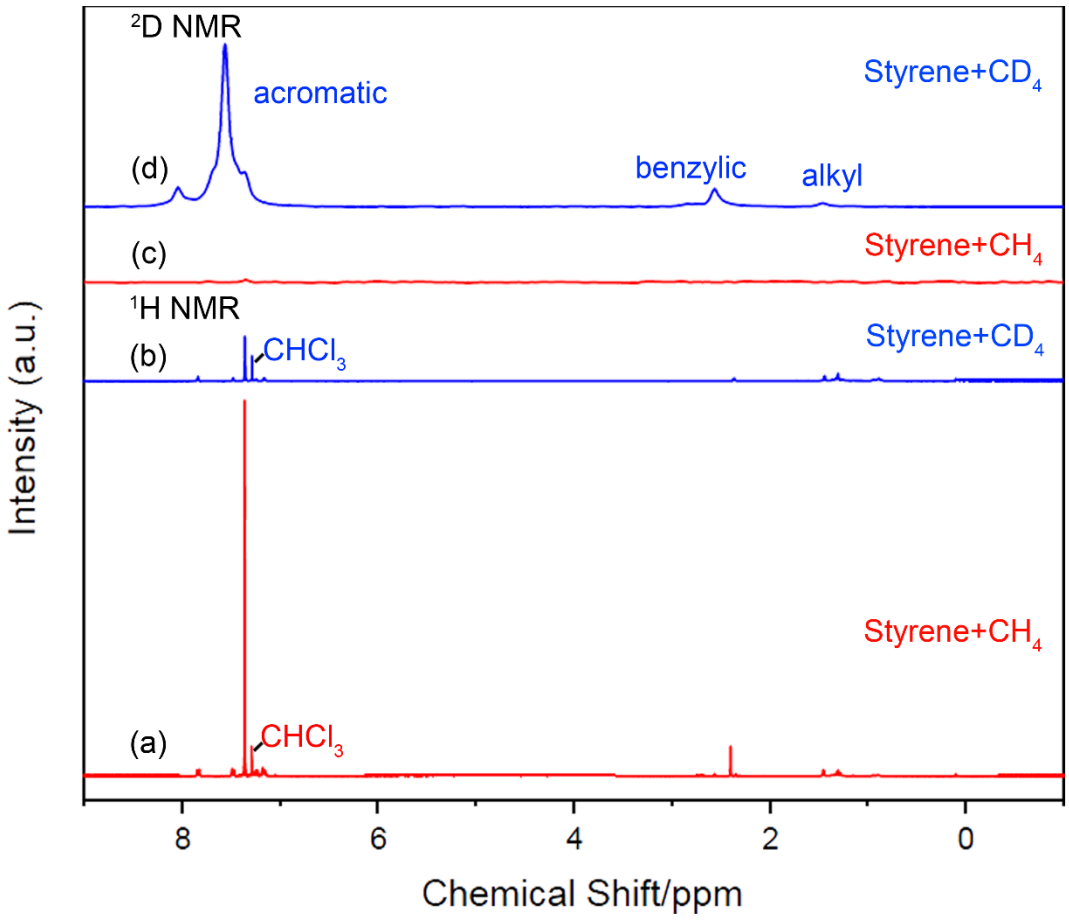

Figure 5. The ^{1}H NMR spectra (a and b) and ^{2}D NMR spectra (c and d) of the liquid products collected from the reaction between styrene and CH_4/CD_4 at 0.3 MPa and 400 ^{o}C for 1 h

Pursuant to the DOE Public Access Plan, this document represents the authors' peer-reviewed, accepted manuscript.
The published version of the article is available from the relevant publisher.

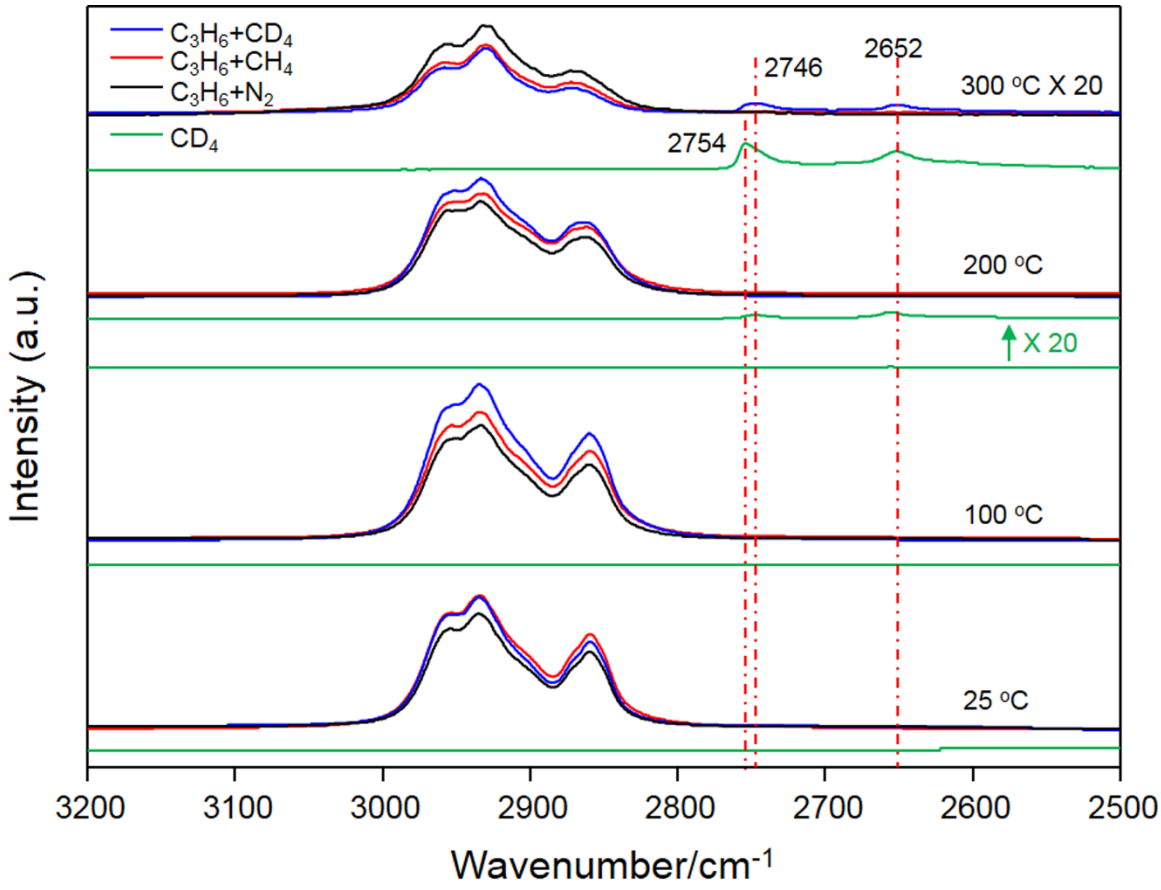

Figure 6. DRIFT spectra acquired upon propylene adsorption over Ag-Ga/ZSM-5 under N_2, CH_4 and CD_4 atmosphere at various temperatures. Spectra acquired under CD_4 without propylene introduction are displayed by the green curves

Pursuant to the DOE Public Access Plan, this document represents the authors' peer-reviewed, accepted manuscript.
The published version of the article is available from the relevant publisher.

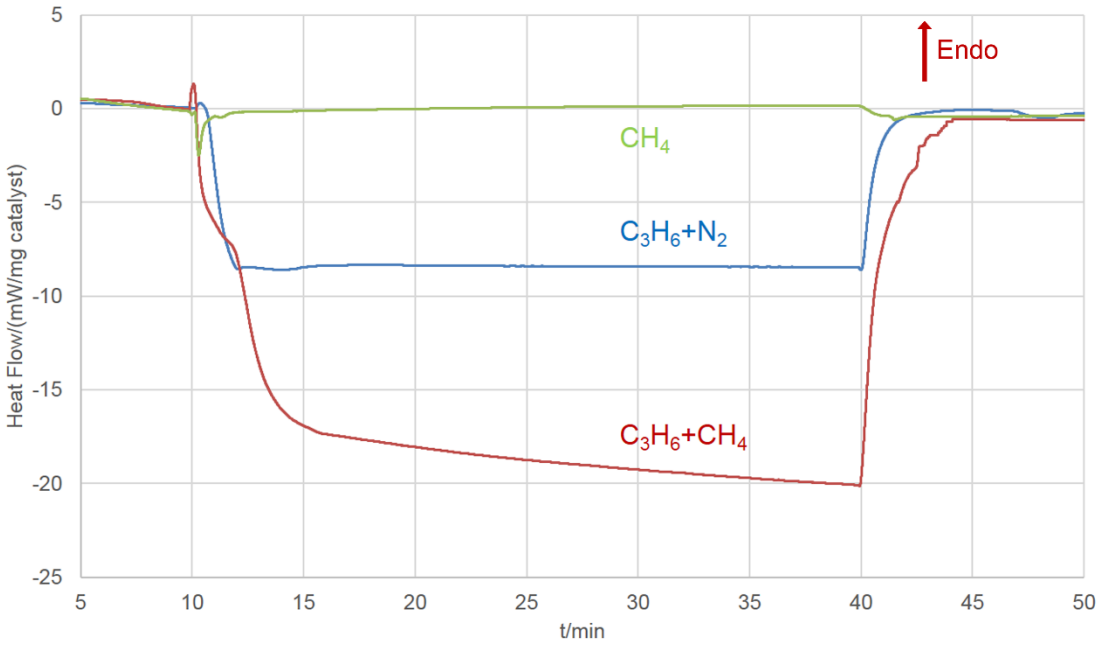

Figure 7. The DSC profiles collected during the reaction of styrene over Ag-Ga/ZSM-5 under various environments and methane-alone run at 400 ^{o}C and 1 atm

Pursuant to the DOE Public Access Plan, this document represents the authors' peer-reviewed, accepted manuscript.
The published version of the article is available from the relevant publisher.

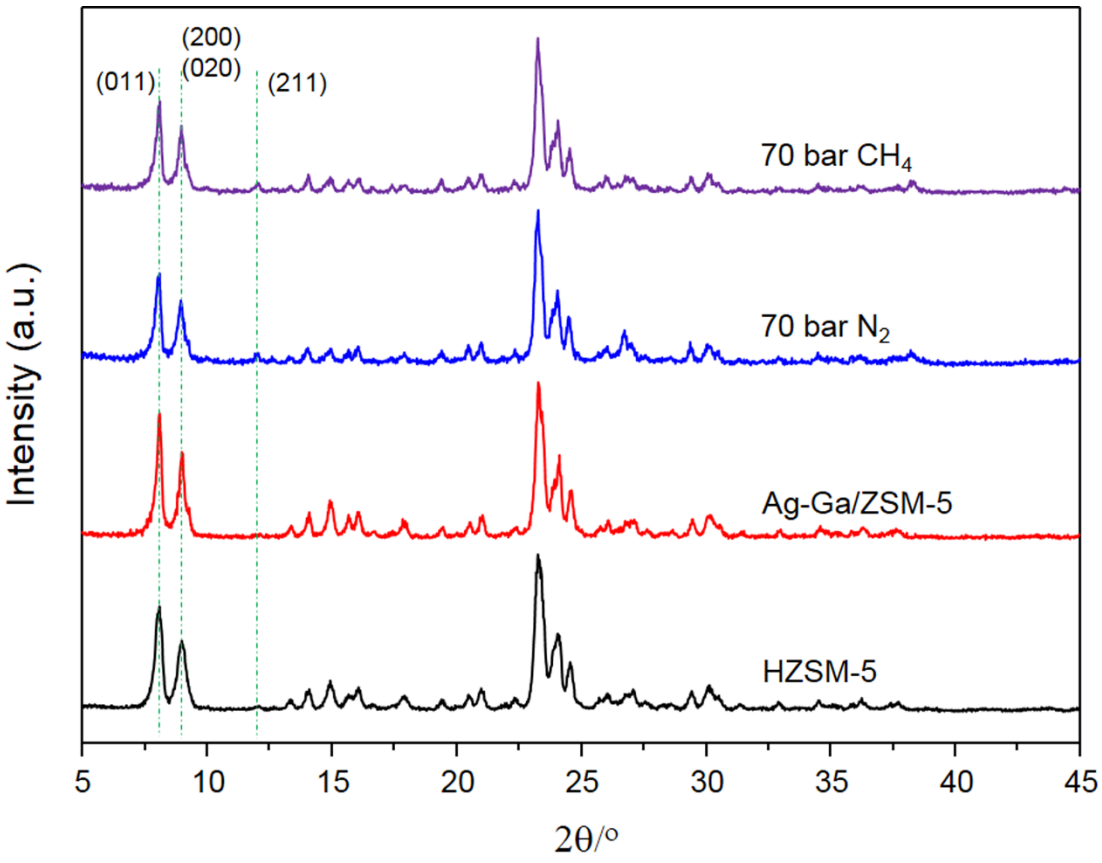

Figure 8. XRD patterns of HZSM-5 and Ag-Ga/ZSM-5 before and after reaction with propylene under various environments at 7.0 MPa and 400 °C for 1h

Pursuant to the DOE Public Access Plan, this document represents the authors' peer-reviewed, accepted manuscript. The published version of the article is available from the relevant publisher.

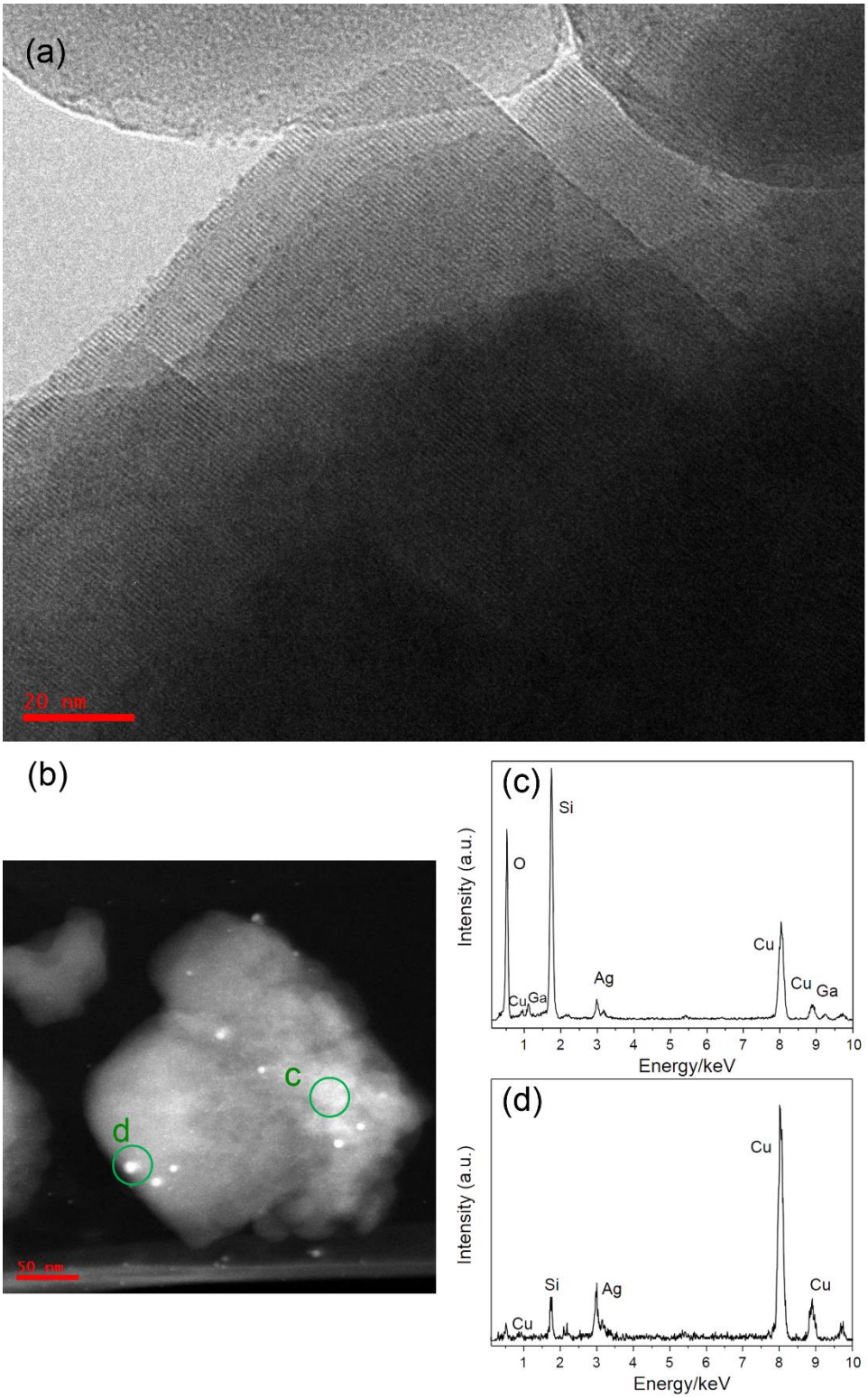

Figure 9. TEM images of fresh Ag-Ga/ZSM-5 in Bright Field (a) and High Angle Annual Dark Field (b), and the EDX spectra (c and d) acquired at the corresponding areas in (b)

Pursuant to the DOE Public Access Plan, this document represents the authors' peer-reviewed, accepted manuscript. The published version of the article is available from the relevant publisher.

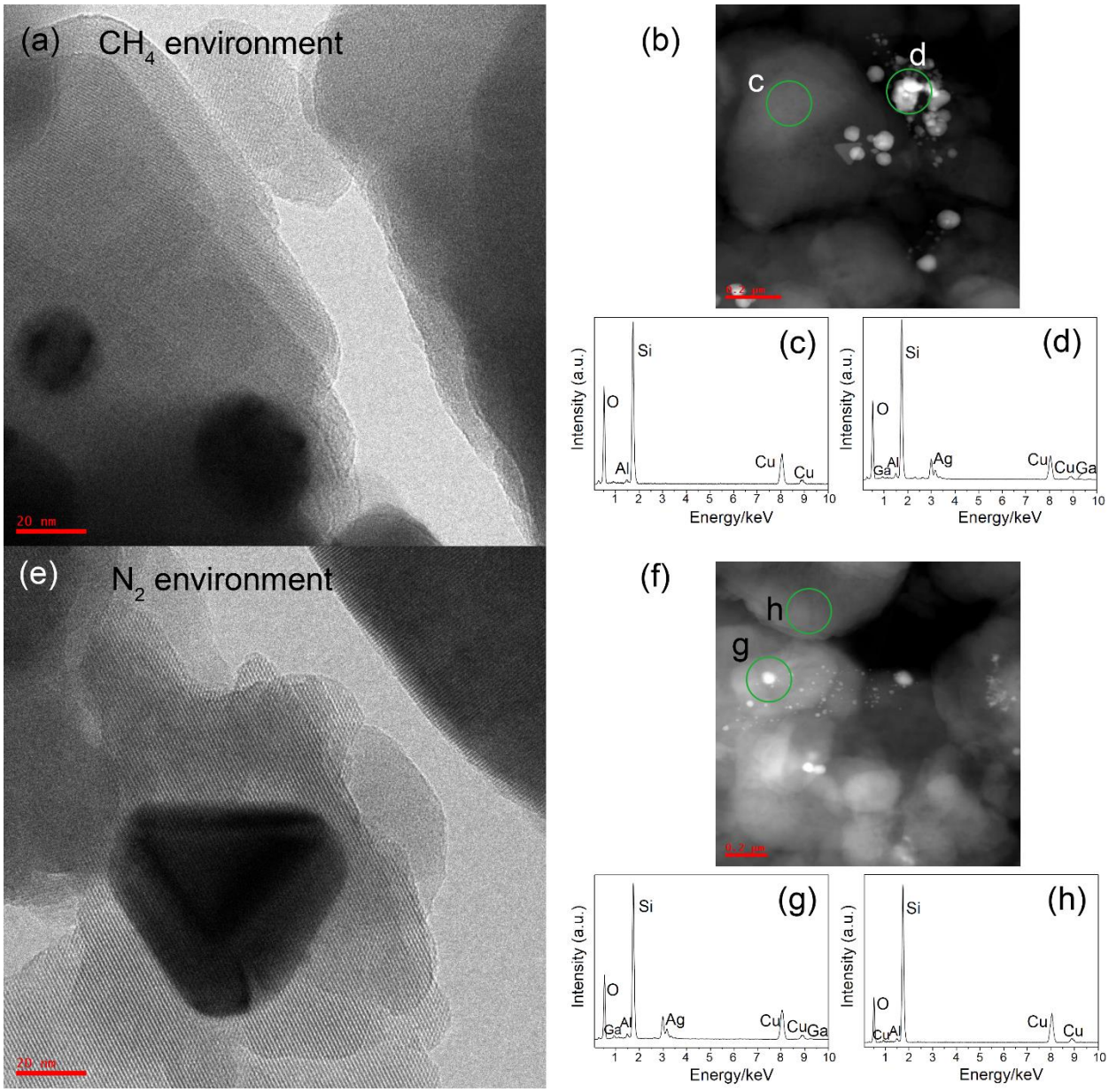

Figure 10. TEM images of spent Ag-Ga/ZSM-5 catalyst collected under CH_4 and N_2 environments at 7.0 MPa in Bright Field (a and e) and High Angle Annual Dark Field (b and f), and the EDX spectra (c, d, g and h) acquired at the corresponding areas in (b and f)

Pursuant to the DOE Public Access Plan, this document represents the authors' peer-reviewed, accepted manuscript. The published version of the article is available from the relevant publisher.

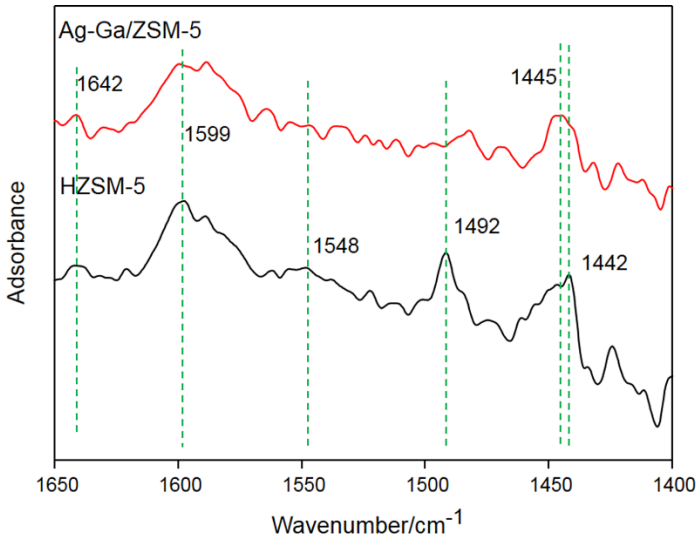

Figure 11. The DRIFT spectra collected over HZSM-5 and Ag-Ga/ZSM-5 upon pyridine adsorption at room temperature

Pursuant to the DOE Public Access Plan, this document represents the authors' peer-reviewed, accepted manuscript. The published version of the article is available from the relevant publisher.

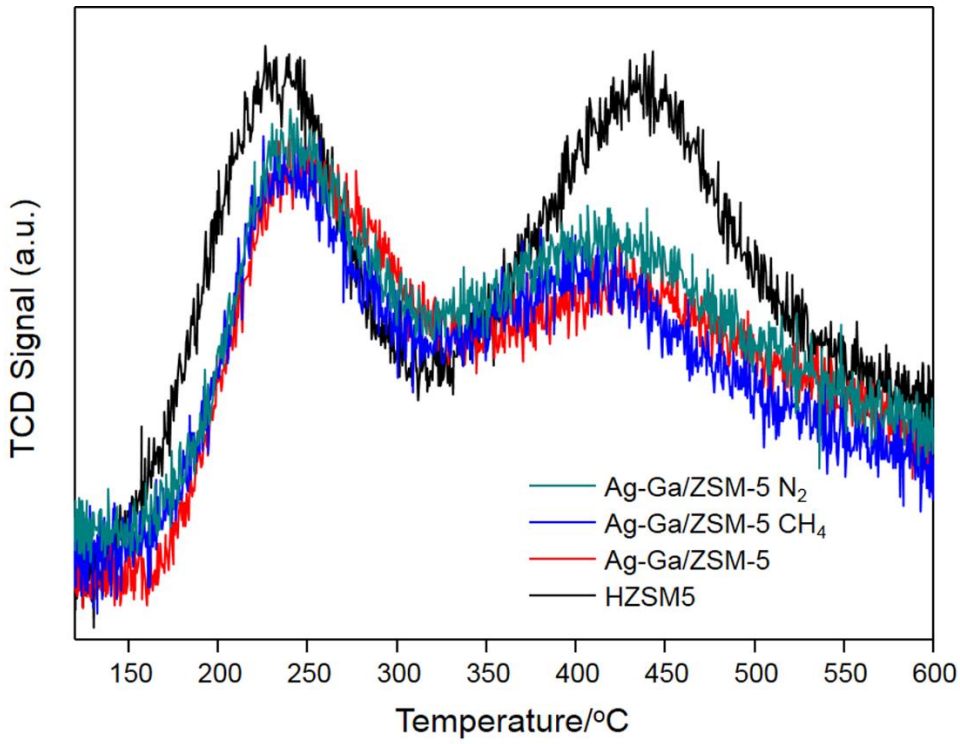

Figure 12. The NH_3-TPD profiles collected over different catalysts

Pursuant to the DOE Public Access Plan, this document represents the authors' peer-reviewed, accepted manuscript.
The published version of the article is available from the relevant publisher.

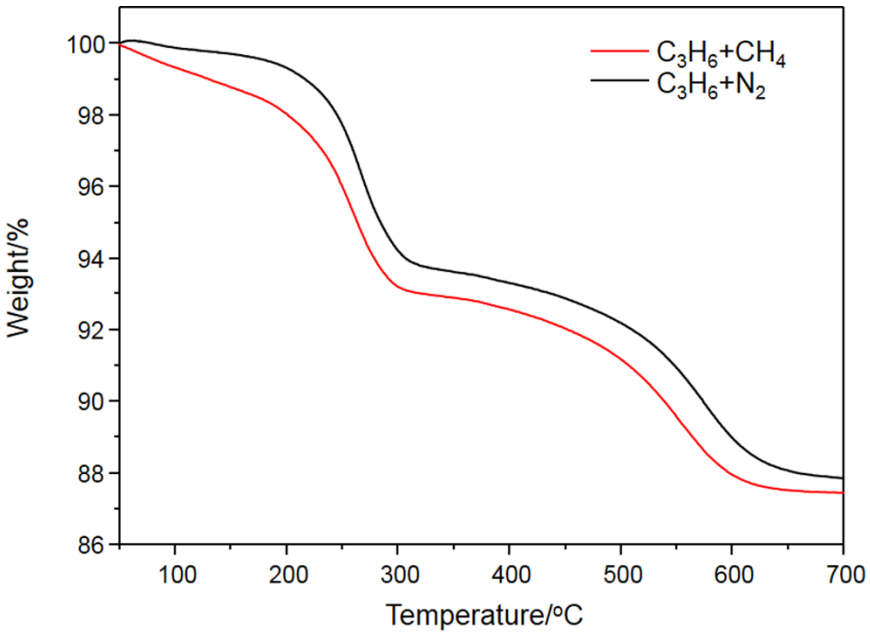

Figure 13. TGA profiles collected over spent Ag-Ga/ZSM-5 after reaction with propylene at 7.0 MPa and 400 °C for 1 h under CH_4 and N_2

Pursuant to the DOE Public Access Plan, this document represents the authors' peer-reviewed, accepted manuscript. The published version of the article is available from the relevant publisher.

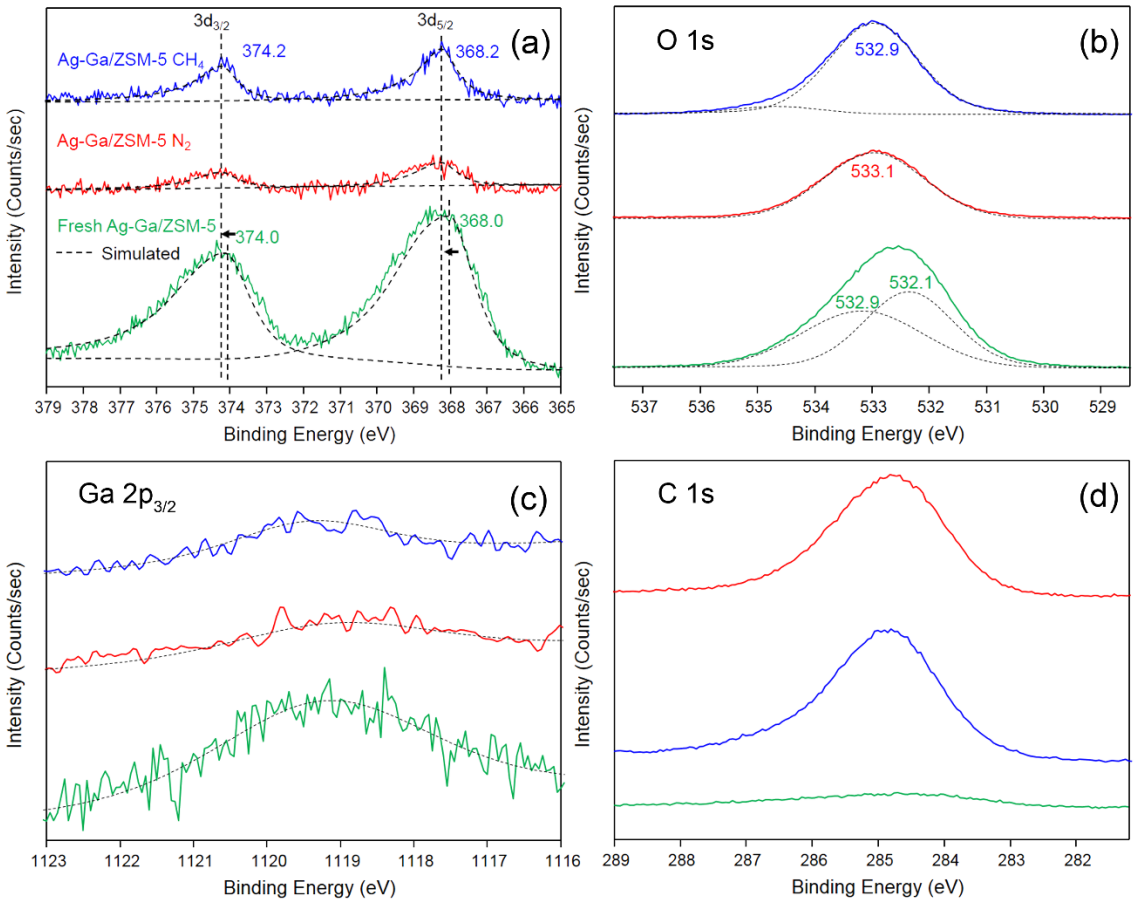

Figure 14. XPS spectra of Ag-Ga/ZSM-5 before and after reaction with propylene at 7.0 MPa and 400 ºC for 1 h under different environments at Ag 3d (a), O 1s (b), Ga $2p_{3/2}$ (c) and C 1s (d) region

Pursuant to the DOE Public Access Plan, this document represents the authors' peer-reviewed, accepted manuscript. The published version of the article is available from the relevant publisher.